

Abstract

A solution of the diffraction from a dielectric-metallic join due to an incident E_z -polarized plane wave is presented. Direct diffraction, coupling, launching, and reflection subproblems associated with a loaded parallel plate waveguide are treated via the dual integral method. The results are subsequently combined in the context of the generalized scattering matrix formulation to obtain the diffraction from the truncated parallel-plate waveguide with a recessed stub and a dielectric loading extending to infinity. The stub is then restored to the waveguide mouth to obtain the diffraction by the dielectric-metallic join. As expected, the final expressions involve several Wiener-Hopf split functions and an efficient numerical technique for their evaluation is given in an appendix. The convergence of the solution with respect to the number of included modes is examined and a number of scattering patterns are presented.

TABLE OF CONTENTS

	<u>Page #</u>
List of Figures	
I. Introduction	1
II. Scattering Matrix Formulation	3
III. Plane Wave Diffraction and Coupling	7
IV. Radiation and Reflection by a Waveguide Mode	20
V. Numerical Results	26
VI. Summary	39
References	41
Appendix A - Expressions for the Split Functions $L_{1,2}(\lambda)$ and $U_{1,2}(\lambda)$	42
Appendix B - An Efficient Numerical Wiener-Hopf Factorization Method	44

LIST OF FIGURES

<u>Figure #</u>	<u>Page #</u>
1. Geometry of the metallic-dielectric join.	2
2. An illustration of stub geometry (a) and associated individual problems. (b) Direct diffraction. (c) Coupling. (d) Reflection from the stub. (e) Reflection at the waveguide mouth. (f) Launching or radiation.	4
3. Illustration of the C and steepest descent path contours in the α -plane along with the chosen branches for the roots $\sqrt{\kappa-\alpha}$ and $\sqrt{\kappa+\alpha}$.	10
4. Mapping of the contours shown in Figure 3 in the α' -plane, where $\cos\alpha = \kappa \cos\alpha'$.	10
5. Illustration of the C contour in the λ -plane, where $\lambda = \cos\alpha$.	14
6. Convergence test of the solution given in equation (1). (a) $2t = 0.95\lambda$, $\epsilon_r = 2$, $\mu_r = 1$. (b) $2t = 0.95\lambda$, $\epsilon_r = 5 - j0.5$, $\mu_r = 1.5 - j0.1$. (c) $2t = 0.95\lambda$, $\epsilon_r = 7.4 - j1.1$, $\mu_r = 1.4 - j0.672$.	27
7. E_z -polarization calculated echowidth family curves for $2t = 0.01, 0.1,$ $0.25, 0.5$ and 0.75 wavelengths. The constitutive parameters of the dielectric are $\epsilon_r = 2$ and $\mu_r = 1$. (a) Backscatter case. (b) Bistatic with $\phi_0 = 45^\circ$. (c) Bistatic with $\phi_0 = 150^\circ$.	30
8. E_z -polarization calculated echowidth family curves for $2t = 0.01, 0.1,$ $0.25, 0.5$ and 0.75 wavelengths. The constitutive parameters of the dielectric are $\epsilon_r = 5 - j0.5$, $\mu_r = 1.4 - j0.1$. (a) Backscatter case. (b) Bistatic, $\phi_0 = 45^\circ$. (c) Bistatic, $\phi_0 = 150^\circ$.	33
9. E_z -polarization calculated echowidth family curves for $2t = 0.01, 0.1,$ $0.25, 0.5$ and 0.75 wavelengths. The constitutive parameters of the dielectric are $\epsilon_r = 7.4 - j1.1$ and $\mu_r = 1.4 - j.672$. (a) Backscatter case. (b) Bistatic, $\phi_0 = 45^\circ$. (c) Bistatic, $\phi_0 = 150^\circ$.	36
B1. Illustration of C_1 contour.	45
B2. Illustration of the C_2 contour with the permitted values of θ .	45

I. Introduction

The problem of interest is the diffraction by a thick metallic-dielectric join illuminated with an E_z -polarized plane wave, as illustrated in Figure 1. To the authors' knowledge, this problem has not been attempted although various researchers have considered related problems. For example, Bates and Mittra [1], and Uchida and Aoki [2] have studied the grounded dielectric slab with a truncated upper plate with regard to surface wave excitation by the dominant parallel-plate waveguide mode. Uchida and Aoki [2], as well as Fong [3], have investigated the radiation cause by the incidence of the dominant waveguide mode upon the waveguide mouth. Also, Aoki and Uchida [4] attempted a solution of the closely related problem of a dielectric-dielectric junction by introducing a Fourier series representation of the field and its derivatives at the interface. Using such an expansion, Wiener-Hopf equations were generated in terms of unknown spectral functions related to the total field. Unfortunately, the authors attempt to obtain an explicit expression for these was not realized. Instead, their computation involves an iterative solution requiring knowledge of rather complex integrals and functions whose evaluation is cumbersome and could only be done approximately.

The dielectric-metallic join problem is of interest primarily as a canonical one in microstrip structures, since a simple application of image theory yields the solution to a dielectric slab recessed in a perfectly conducting ground plane. Further impetus is derived when one considers the presence of composite materials on man-made structures where the occurrence of material-metallic junctions is common place.

The solution to the diffraction by the metallic-dielectric join is obtained by first considering the closely allied problem of a parallel-plate waveguide with a dielectric loading extending to infinity and a perfectly conducting stub recessed a distance from the waveguide mouth as shown in Figure 2a. Upon a solution of this, it is then a simple matter to extract the solution for the metallic-dielectric join by setting the distance d to zero. The diffraction of the

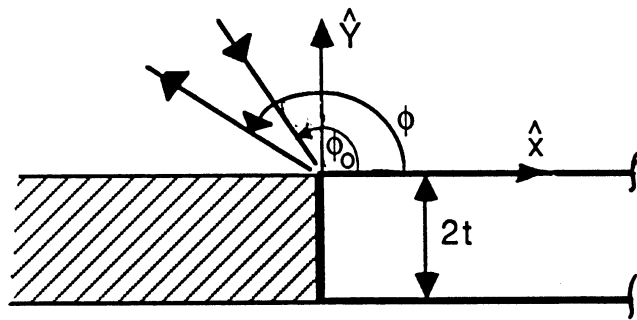


Fig. 1. Geometry of the metallic-dielectric join.

recessed-stub geometry due to an incident plane wave is treated in the context of the generalized scattering matrix formulation (GSMF) [5]. This method requires a solution to a number of canonical problems, illustrated in Figures 2b-2f. Specifically, in addition to the direct diffraction problem, one must also consider the coupling, reflection, and launching of waveguide modes at the loaded waveguide mouth. Each of these will be analyzed via the dual integral equation approach [6], which provides a reduction in complexity over the parallel Wiener-Hopf technique. A crucial step in every one of these problems is the factorization of a particular complex function into components regular in the upper and lower half complex plane. Unfortunately, the factorization cannot be done analytically and to circumvent this difficulty an efficient numerical method is introduced for the factorization of an arbitrary even complex function.

In the first part of this report, the formal solution to the problem is presented. After a short summary of the GSMF, the integral equations for E_z -polarization incidence are formulated in a consistent manner by imposing the necessary boundary conditions. The coupling and direct diffraction coefficients, as well as the launching and reflection coefficients are then extracted from a solution of the appropriate integral equations last presented. In the final part of the report, families of computed scattering patterns are presented for selected material parameters to illustrate the scattering behavior of the dielectric-metallic join as a function of slab thickness. The convergence behavior of the formal solution is also examined with respect to the included number of modes.

II. Scattering Matrix Formulation

The problem to be considered is that of an E_z -polarized plane wave incident upon the structure shown in Figure 1. In order to apply the GSMF procedure, the stub must be recessed a distance d into the waveguide, as shown in Figure 2a, forming the genesis of the

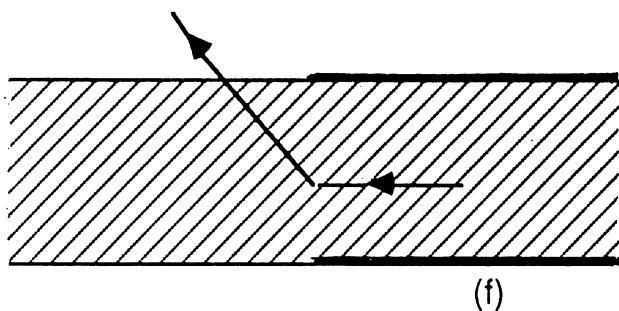
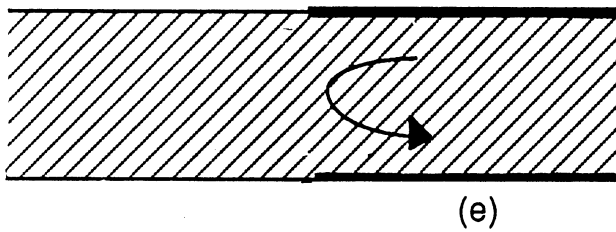
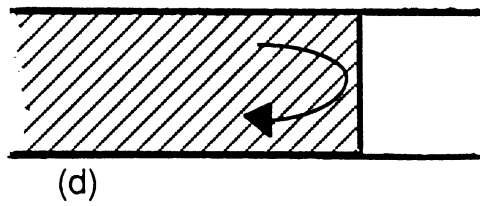
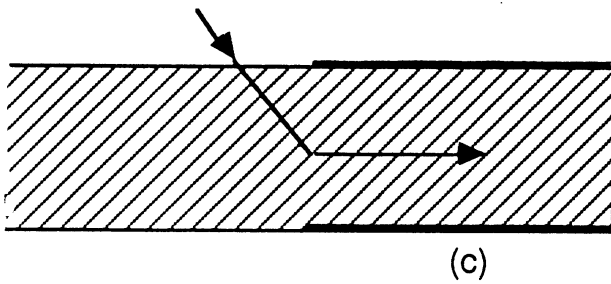
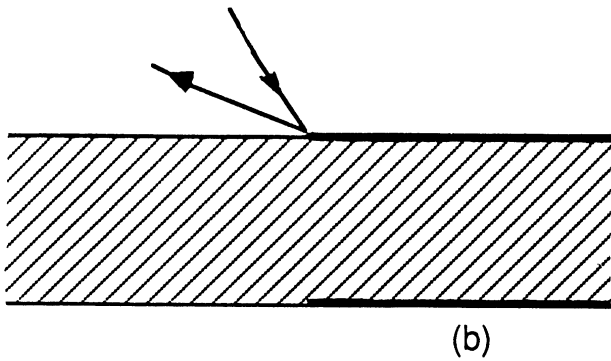
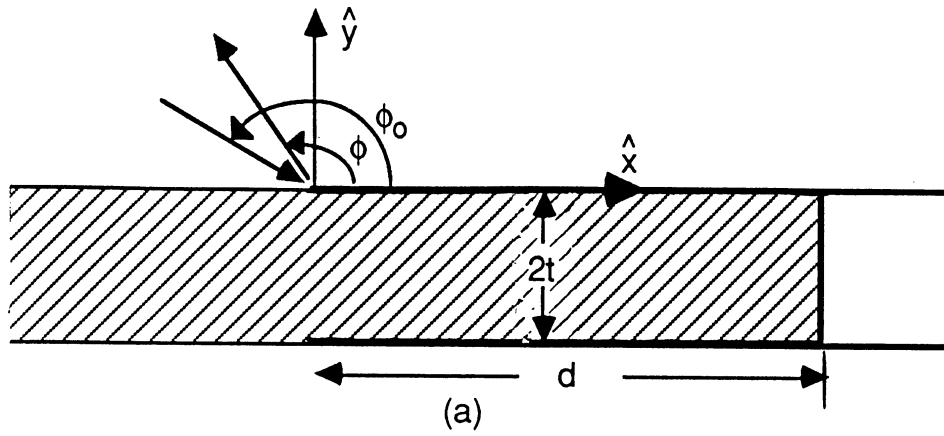


Fig. 2. Illustration of stub geometry (a) and associated individual problems: (b) Direct diffraction. (c) Coupling. (d) Reflection from the stub. (e) Reflection at the waveguide mouth. (f) Launching or radiation.

individual problems illustrated in Figures 2b-2f. At the end of the procedure, the distance d is set to zero restoring the original geometry.

In accordance with the GSMF, the individual problems to be considered are as follows:

1) Evaluation of the direct diffracted field by the substructure in Figure 2b due to plane wave incidence. This field will be denoted as

$$E_{DD}(\phi, \phi_o) \sim S_{DD}(\phi, \phi_o) \frac{e^{-jk\rho}}{\sqrt{\rho}}$$

where S_{DD} is usually referred to as the diffraction coefficient and (ρ, ϕ) are the cylindrical coordinates of the far zone observation point.

2) Evaluation of the field coupled into the loaded parallel-plate waveguide due to plane wave incidence as shown in Figure 2c. Hereon we will denote the field associated with the n th coupled mode as

$$E_{Cn}(\phi_o) = C_n(\phi_o) e^{-jk_n x}$$

where $C_n(\phi_o)$ is usually referred to as the coupling coefficient and k_n is the propagation constant associated with the n th mode.

3) Evaluation of the modal field reflected at the stub. This will be written as $\Gamma_{mn} e^{jk_m x}$ where Γ_{mn} is the stub reflection coefficient of the n th mode to the m th mode.

4) Evaluation of the reflected field at the waveguide mouth due to the n th mode. This will be denoted as $R_{mn} e^{-jk_m x}$ where R_{mn} is the reflection coefficient of the n th mode to the m th mode.

5) Evaluation of the far-zone radiated field due to an incident n th mode at the waveguide mouth. This field will be denoted as

$$E_{L_n}(\phi) \sim L_n(\phi) \frac{e^{-jk\rho}}{\sqrt{\rho}}$$

where $L_n(\phi)$ is usually referred to as the launching coefficient associated with the n th waveguide mode.

Accordingly, the total far-zone diffracted field by the recessed stub geometry in Figure 2a is given by

$$E_z^s(\phi, \phi_o; d) \sim \left[S_{DD}(\phi, \phi_o) + S_{MOD}(\phi, \phi_o; d) \right] \frac{e^{-jk\rho}}{\sqrt{\rho}} \quad (1)$$

where $S_{MOD}(\phi, \phi_o; d)$ is associated with the presence of the stub and, therefore, includes the contribution of the modal fields within the waveguide. It can be written in a matrix form as [7]

$$S_{MOD}(\phi, \phi_o; d) = [L_m(\phi)]^T \left\{ [I] - [P_{mn}] [\Gamma_{mn}] [P_{mn}] [R_{mn}] \right\}^{-1} [P_{mn}] [\Gamma_{mn}] [P_{mn}] [C_n(\phi)] \quad (2)$$

in which the brackets signify column or square matrices depending on whether one or two subscripts appear, respectively. In addition, $[I]$ denotes the identity matrix and $[P_{mn}]$ is the modal propagation matrix whose elements are given by

$$P_{mn} = \begin{cases} e^{-jk_m d} & ; \quad m = n \\ 0 & ; \quad m \neq n \end{cases} \quad (3)$$

Clearly to obtain the far-zone scattered field by the dielectric-metallic join it is only required to set $d = 0$ in (1) and (2). In this case $[P_{mn}]$ reduces to the identity matrix and

$S_{MOD}(\phi, \phi_o)$ becomes

$$S_{\text{MOD}}(\phi, \phi_o) \equiv S_{\text{MOD}}(\phi, \phi_o; 0) = [L_m(\phi)]^T \left\{ [I] - [\Gamma_{mn}] [R_{mn}] \right\}^{-1} [\Gamma_{mn}] [C_n(\phi)] . \quad (4)$$

III. Plane Wave Diffraction and Coupling

The plane wave (an $e^{j\omega t}$ convention is assumed and suppressed throughout)

$$\begin{aligned} E_z^i &= e^{jk(x \cos\phi_o + y \sin\phi_o)} \\ H_x^i &= -Y \sin\phi_o e^{jk(x \cos\phi_o + y \sin\phi_o)} \\ H_y^i &= +Y \sin\phi_o e^{jk(x \cos\phi_o + y \sin\phi_o)} \end{aligned} \quad (5)$$

is assumed to be incident upon the structure in Figure 2b, where $Y = 1/Z$ is the free space admittance and ϕ_o is the angle of incidence measured from the positive x-axis.

In the absence of the perfectly conducting half-planes, the plane wave (5) will produce the following total field

$$E_z^{\text{pw}} = \begin{cases} E_z^i + E_z^r & y > 0 \\ E_z^m & 0 > y > -2t \\ E_z^{\text{tr}} & y < -2t \end{cases} , \quad (6)$$

where

$$E_z^r = R_E e^{jk(x \cos\phi_o - y \sin\phi_o)} \quad (7a)$$

$$E_z^m = e^{jkx \cos\phi_o} \left[\frac{(1 + R_E) \sin[k'(y + 2t) \sin\phi_o'] - T_E \sin(k' y \sin\phi_o') e^{-j2kt \sin\phi_o}}{\sin(2k' t \sin\phi_o')} \right] \quad (7b)$$

$$E_z^{tr} = T_E e^{jk(x \cos\phi_o + y \sin\phi_o)}, \quad (7c)$$

$$R_E = \frac{R_{EO}(1 - P_b^2 P_a)}{1 - R_{EO}^2 P_b^2 P_a}, \quad T_E = \frac{(1 - R_{EO}^2) P_b P_c}{1 - R_{EO}^2 P_b^2 P_a} \quad (8)$$

$$P_a = e^{j4kt \cos\phi_o \cot\phi_o'}, \quad P_b = e^{-j2k' t/\sin\phi_o'}, \quad P_c = e^{j2kt \cos(\phi_o - \phi_o')/\sin\phi_o'} \quad (9)$$

and R_{EO} is the usual plane wave reflection coefficient associated with a dielectric half-space

having relative constitutive parameters ϵ_r and μ_r . In addition

$$k' = k \sqrt{\mu_r \epsilon_r} = \kappa k, \quad (10)$$

where κ is the refraction index and ϕ_o' is defined according to Snell's law as

$$k \cos\phi_o = k' \cos\phi_o'. \quad (11)$$

The presence of the perfectly conducting half-plane causes the generation of the additional field

$$E_z^s = \begin{cases} E_{z1}^s & y > 0 \\ E_{z2}^s & -2t < y < 0 \\ E_{z3}^s & y < -2t. \end{cases} \quad (12)$$

These may be represented in terms of an angular spectrum of plane waves [6]. Specifically, a suitable spectral representation for them takes the form

$$E_{z1}^s = \int_C P_1(\cos\alpha) e^{-jk\rho \cos(\phi - \alpha)} d\alpha \quad , \quad (13a)$$

$$E_{z2}^s = \int_C \left[Q_1(\cos\alpha) e^{-jk'\rho \cos(\phi + \alpha')} + Q_2(\cos\alpha) e^{-j2k't \sin\alpha'} e^{-jk'\rho \cos(\phi - \alpha)} \right] d\alpha \quad , \quad (13b)$$

$$E_{z3}^s = \int_C P_2(\cos\alpha) e^{j2kt \sin\alpha} e^{-jk\rho \cos(\phi + \alpha)} d\alpha \quad . \quad (13c)$$

where C is the contour on which $\cos\alpha$ runs from $+\infty$ to $-\infty$ as shown in Figure 3 and $P_{1,2}(\cos\alpha)$ with $Q_{1,2}(\cos\alpha)$ are the spectra which must be determined via the application of the necessary boundary conditions. Note also that α and α' are different parameters whose relationship will be established later. The introduction of the factors $e^{j2kt \sin\alpha}$ and $e^{-j2k't \sin\alpha'}$ is totally arbitrary and could have been omitted. However, such factors are expected to appear in the final expressions for the spectra and are therefore introduced from the start in order to reduce the complexity of the resulting integral equations. The corresponding expressions for the x-component of the scattered magnetic field are

$$H_{x1}^s = Y \int_C \sin\alpha P_1(\cos\alpha) e^{-jk\rho \cos(\phi - \alpha)} d\alpha \quad , \quad (14a)$$

$$H_{x2}^s = -Y' \int_C \sin\alpha' \left[Q_1(\cos\alpha) e^{-jk'\rho \cos(\phi + \alpha')} - Q_2(\cos\alpha) e^{-j2k't \sin\alpha'} e^{-jk'\rho \cos(\phi - \alpha')} \right] d\alpha \quad , \quad (14b)$$

$$H_{x3}^s = -Y \int_C \sin\alpha P_2(\cos\alpha) e^{j2kt \sin\alpha} e^{-jk\rho \cos(\phi + \alpha)} d\alpha \quad , \quad (14c)$$

where

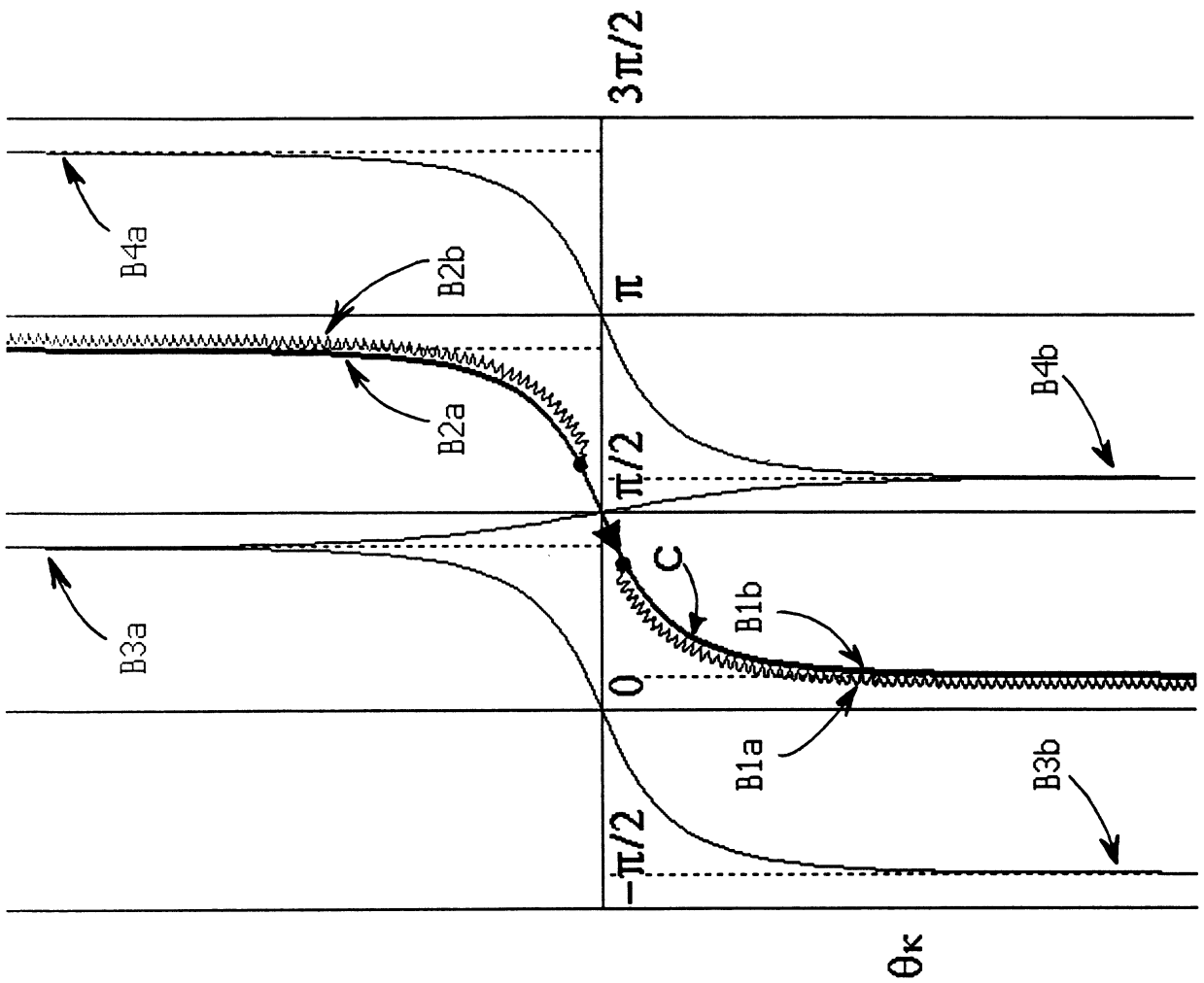


Fig. 4. Mapping of the contours shown in

Fig. 3 in the α' -plane, where $\cos\alpha = \kappa \cos\alpha'$.

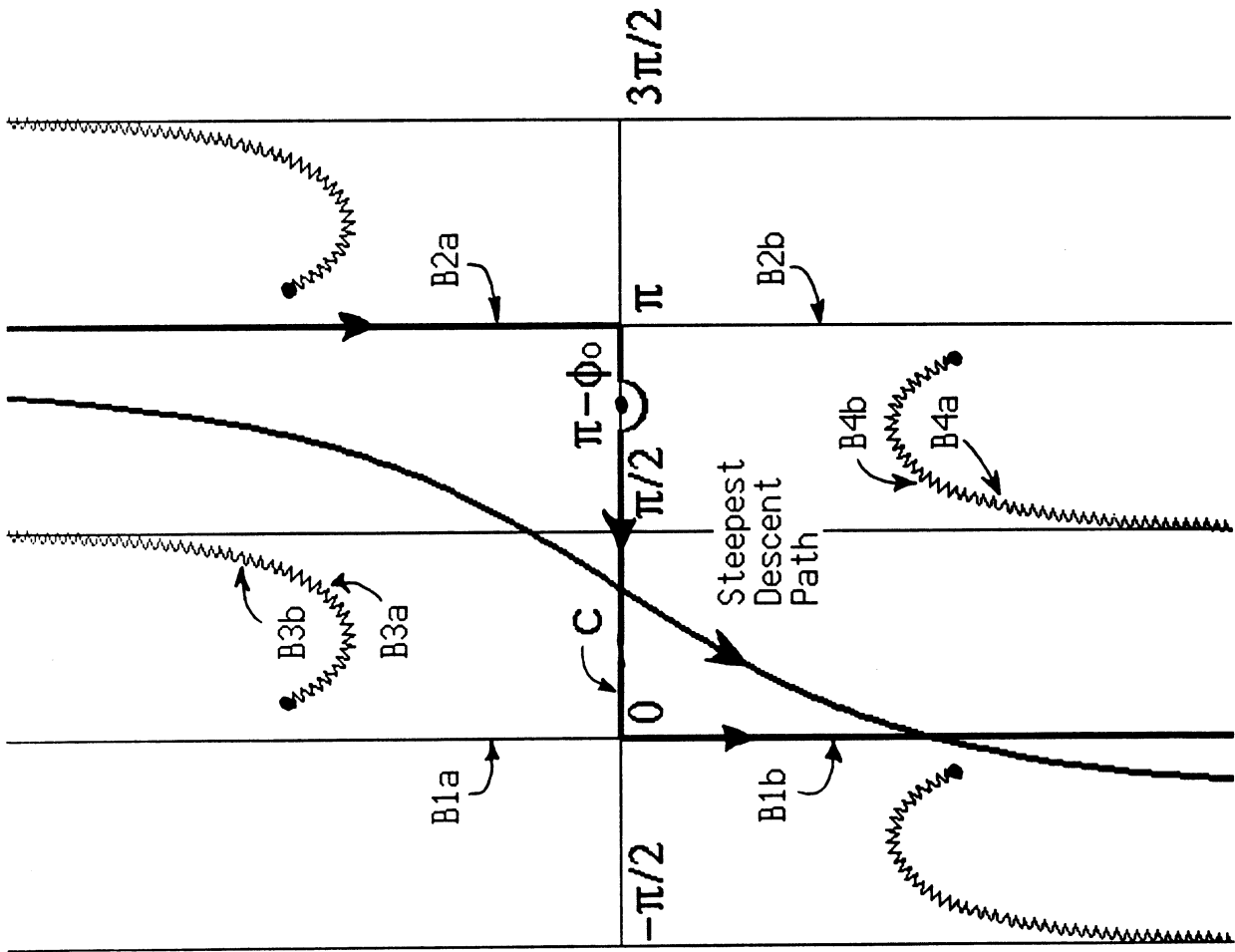


Fig. 3. Illustration of the C and steepest descent path contours in the α -plane along with the chosen branches for the roots $\sqrt{\kappa-\alpha}$ and $\sqrt{\kappa+\alpha}$.

$$Y = \sqrt{\frac{\epsilon_r}{\mu_r}} Y = Y_n Y .$$

The total field due to a plane wave incidence in the presence of the configuration in Figure 2b can now be expressed as

$$E_z^{\text{tot}} = E_z^{\text{pw}} + E_z^{\text{s}} , \quad (15)$$

with E_z^{pw} and E_z^{s} as defined in (6) and (12) respectively. For its complete determination we must find the scattered field E_z^{s} , implying an explicit knowledge of the angular spectra $P_{1,2}(\cos\alpha)$ and $Q_{1,2}(\cos\alpha)$ appearing in (13). This will be accomplished in the subsequent sections via the application of the following boundary conditions:

1) The total tangential electric field is continuous over $-\infty < x < \infty$, $y = \begin{Bmatrix} 0 \\ -2t \end{Bmatrix}$, implying

$$(B1) \quad E_{z1}^{\text{s}} = E_{z2}^{\text{s}} \quad \text{over } -\infty < x < \infty, \quad y = 0 ,$$

$$(B2) \quad E_{z2}^{\text{s}} = E_{z3}^{\text{s}} \quad \text{over } -\infty < x < \infty, \quad y = -2t ,$$

since E_z^{pw} is already continuous.

2) The total tangential magnetic field is continuous over $x < 0$, $y = \begin{Bmatrix} 0 \\ -2t \end{Bmatrix}$, implying

$$(B3) \quad H_{x1}^{\text{s}} = H_{x2}^{\text{s}} \quad \text{over } x < 0, \quad y = 0 ,$$

$$(B4) \quad H_{x2}^{\text{s}} = H_{x3}^{\text{s}} \quad \text{over } x < 0, \quad y = -2t .$$

3) The tangential electric field vanishes on the perfectly conductive half-planes, implying

$$(B5) \quad E_z^{\text{i}} + E_z^{\text{r}} + E_{z1}^{\text{s}} = 0 \quad \text{over } x > 0, \quad y = 0 ,$$

$$(B6) \quad E_z^{\text{tr}} + E_{z3}^{\text{s}} = 0 \quad \text{over } x > 0, \quad y = -2t .$$

The application of boundary conditions (B1) - (B2) gives

$$k \cos \alpha = k' \cos \alpha' \text{ or } k' \sin \alpha' = k \sqrt{\kappa^2 - \cos^2 \alpha} \text{ ,} \quad (16)$$

and that

$$P_{\frac{1}{2}}(\cos \alpha) = Q_{\frac{1}{2}}(\cos \alpha) + Q_{\frac{2}{1}}(\cos \alpha) e^{-j2k't} \sqrt{\kappa^2 - \cos^2 \alpha} \text{ .} \quad (17)$$

Thus, (17) reduces the number of unknown spectra from four to two and a complete

knowledge of the scattered fields can be deduced from $Q_{1,2}(\cos \alpha)$ alone. Additionally, the

branch of $\sqrt{\kappa^2 - \cos^2 \alpha}$ in (16) is chosen such that $\text{Im} \left(\sqrt{\kappa^2 - \cos^2 \alpha} \right) < 0$ for $0 \leq \text{Re}(\alpha) \leq \pi$. This

defines a mapping from the α -plane to the α' -plane as shown in Figure 4.

Next we employ the boundary conditions (B3) - (B4) demanding that

$$\int_C \left[\sin \alpha P_1(\cos \alpha) + Y_n \sin \alpha' Q_1(\cos \alpha) - Y_n \sin \alpha' Q_2(\cos \alpha) e^{-j2k't} \sin \alpha' \right] e^{-jkx \cos \alpha} d\alpha = 0; \quad (18a)$$

$x < 0 \text{ ,}$

$$\int_C \left[\sin \alpha P_2(\cos \alpha) - Y_n \sin \alpha' Q_1(\cos \alpha) e^{-j2k't} \sin \alpha' + Y_n \sin \alpha' Q_2(\cos \alpha) \right] e^{-jkx \cos \alpha} d\alpha = 0; \quad (18b)$$

$x < 0 \text{ .}$

When we further incorporate (17) into (18), change the variable of integration from α to

$\lambda = \cos \alpha$ and add and subtract the resulting equations we obtain the decoupled set

$$\int_{-\infty}^{\infty} [Q_1(\lambda) \pm Q_2(\lambda)] \frac{\sqrt{\kappa^2 - \lambda^2}}{\sqrt{1 - \lambda^2}} F_3(\lambda) e^{-jkx\lambda} d\lambda = 0; \quad x < 0 \text{ ,} \quad (19)$$

where

$$F_3(\lambda) = \frac{2 \left[\mu_r \sqrt{\lambda^2 - 1} \cosh \left(kt \sqrt{\lambda^2 - \kappa^2} \right) + \sqrt{\lambda^2 - \kappa^2} \sinh \left(kt \sqrt{\lambda^2 - \kappa^2} \right) \right]}{(\mu_r + 1) \sqrt{\lambda^2 - \kappa^2} e^{kt \sqrt{\lambda^2 - \kappa^2}}}, \quad (20a)$$

and

$$F_4(\lambda) = \frac{2 \left[\mu_r \sqrt{\lambda^2 - 1} \sinh \left(kt \sqrt{\lambda^2 - \kappa^2} \right) + \sqrt{\lambda^2 - \kappa^2} \cosh \left(kt \sqrt{\lambda^2 - \kappa^2} \right) \right]}{(\mu_r + 1) \sqrt{\lambda^2 - \kappa^2} e^{kt \sqrt{\lambda^2 - \kappa^2}}}. \quad (20b)$$

Note that in deriving (16) we have used the relations $\sqrt{\lambda^2 - 1} = j \sqrt{1 - \lambda^2}$ and $\sqrt{\lambda^2 - \kappa^2} = j \sqrt{\kappa^2 - \lambda^2}$.

In addition, the complex λ -plane defined by the mapping $\lambda = \cos \alpha$ is shown in Figure 5.

The boundary conditions (B5) and (B6) imply the integral equations

$$\int_{-\infty}^{\infty} \frac{1}{\sqrt{1 - \lambda^2}} P_1(\lambda) e^{-jkx\lambda} d\lambda = -(1 + R_E) e^{jkx \cos \phi_0} \quad ; x > 0, \quad (21a)$$

$$\int_{-\infty}^{\infty} \frac{1}{\sqrt{1 - \lambda^2}} P_2(\lambda) e^{-jkx\lambda} d\lambda = -T_E e^{-j2kt \sin \phi_0} e^{jkx \cos \phi_0} \quad ; x > 0. \quad (21b)$$

Substituting (17) into (21) and adding and subtracting the resulting equations we find

$$\int_{-\infty}^{\infty} [Q_1(\lambda) \pm Q_2(\lambda)] \frac{1}{\sqrt{1 - \lambda^2}} F_1(\lambda) e^{-jkx\lambda} d\lambda = -(1 + R_E \pm T_E e^{-j2kt \sin \phi_0}) e^{jkx \cos \phi_0} \quad ; x > 0, \quad (22)$$

with

$$F_1(\lambda) = 1 \pm e^{-j2kt \sqrt{\kappa^2 - \lambda^2}}. \quad (23)$$

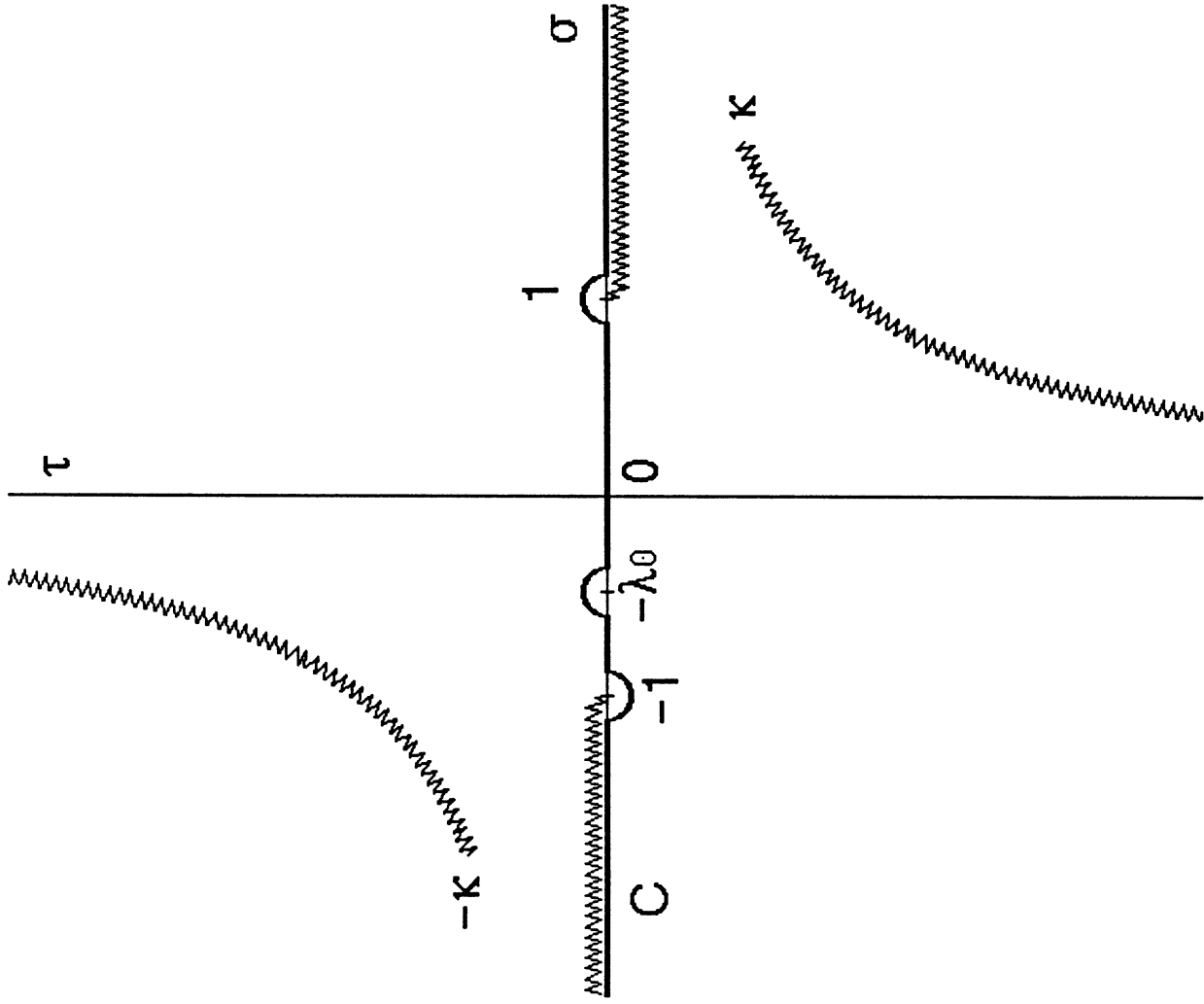


Fig. 5. Illustration of the C contour in the λ -plane,
 where $\lambda = \cos \alpha$.

The dual integral equations (19) and (22) are now sufficient for a solution of

$Q_1(\lambda) \pm Q_2(\lambda)$. However, before such a solution can be pursued, it is necessary that

$F_{1,2}(\lambda)$ and $F_{3,4}(\lambda)$ be factorized into functions regular (i.e. free of poles, zeros and branch points) in the upper and lower half of the complex λ -plane. Utilizing the factorization

procedure outlined in Noble [8], $F_{1,2}(\lambda)$ may be factorized as

$$F_{1,2}(\lambda) = L_{1,2}(\lambda) U_{1,2}(\lambda) \quad , \quad (24)$$

where the functions denoted by L/U are regular in the upper/lower half of the λ -plane.

Expressions for $L_{1,2}(\lambda)$, $U_{1,2}(\lambda)$ are given in Appendix A. On the other hand, the

factorization of $F_{3,4}(\lambda)$ into

$$F_{3,4}(\lambda) = L_{3,4}(\lambda) U_{3,4}(\lambda) \quad , \quad (25)$$

is much more involved. Notwithstanding, numerical and analytical techniques do exist for

accomplishing it [1,9]. The factorization of $F_{3,4}(\lambda)$ herein will be accomplished through a

recently developed numerical procedure with the final expressions of $U_{3,4}(\lambda)$ and $L_{3,4}(\lambda)$ in

terms of an integral over the convenient finite interval $[0,1]$, as given in Appendix B. The

utility of this numerical technique also stems from the fact that it may be applied to a very

wide class of complex functions with no special preconditioning of these necessary (i.e.

involved treatment of poles, etc.). In passing, we note that for the special case of $\kappa = 1$,

$F_{1,2}(\lambda)$ reduce to functions already encountered [10] and $F_{3,4}(\lambda) = 1$.

Using the factorizations (24) and (25) we may now proceed for a solution of the spectra $Q_{1,2}$. Since (19) holds for $x < 0$, we may close the path of integration by a

semi-infinite contour in the upper half of the λ -plane and employ Cauchy's theorem along with (25) to deduce that

$$[Q_1(\lambda) \pm Q_2(\lambda)] \frac{\sqrt{\kappa^2 - \lambda^2}}{\sqrt{1 - \lambda^2}} L_3(\lambda) U_3(\lambda) = U_{A,B}(\lambda) \quad (26)$$

where $U_{A,B}(\lambda)$ are unknown functions regular in the upper half of the λ -plane. Similarly, (22) holds for $x > 0$ enabling us to close the path of integration by a semi-infinite contour in the lower half of the λ -plane and again invoke Cauchy's theorem along with (24) to obtain

$$[Q_1(\lambda) \pm Q_2(\lambda)] \frac{1}{\sqrt{1 - \lambda^2}} L_1(\lambda) U_1(\lambda) = \frac{1}{2\pi j} \frac{(1 + R_E \pm T_E e^{-j2kt \sin\phi_0})}{\lambda + \cos\phi_0} \frac{L_{A,B}(\lambda)}{L_{A,B}(-\cos\phi_0)}, \quad (27)$$

where $L_{A,B}(\lambda)$ are unknown functions regular in the lower half λ -plane. Substituting (26) into (27) it may be deduced that

$$L_{A,B}(\lambda) = \frac{-L_1(\lambda)}{L_3(\lambda) \sqrt{\kappa + \lambda}}, \quad (28)$$

$$U_{\frac{A}{B}}(\lambda) = \frac{1}{2\pi j} (1 + R_E \pm T_E e^{-j2kt \sin\phi_0}) \frac{\sqrt{\kappa - \lambda_0} \sqrt{\kappa - \lambda}}{\lambda + \lambda_0} \frac{U_4(\lambda_0) U_4(\lambda)}{U_1(\lambda_0) U_1(\lambda)}, \quad (29)$$

since $L_{A,B}$ and $U_{A,B}$ are associated with different regions of regularity. Finally from (29) and (26) it follows that

$$Q_{\frac{1}{2}}(\lambda) = \frac{1}{4\pi j} \frac{\sqrt{1+\lambda}}{\sqrt{\kappa+\lambda}} \frac{\sqrt{1-\lambda} \sqrt{\kappa-\lambda_0}}{\lambda+\lambda_0} \left\{ (1 + R_E + T_E e^{-j2kt \sin\phi_0}) \frac{U_3(\lambda_0)}{L_3(\lambda) U_1(\lambda) U_1(\lambda_0)} \right. \\ \left. \pm (1 + R_E - T_E e^{-j2kt \sin\phi_0}) \frac{U_4(\lambda_0)}{L_4(\lambda) U_2(\lambda) U_2(\lambda_0)} \right\}, \quad (30)$$

and from (17)

$$P_{\frac{1}{2}}(\lambda) = \frac{1}{4\pi j} \frac{\sqrt{1+\lambda}}{\sqrt{\kappa+\lambda}} \frac{\sqrt{1-\lambda} \sqrt{\kappa-\lambda_0}}{\lambda+\lambda_0} \left\{ (1 + R_E + T_E e^{-j2kt \sin\phi_0}) \frac{L_1(\lambda) U_3(\lambda_0)}{L_3(\lambda) U_1(\lambda_0)} \right. \\ \left. \pm (1 + R_E - T_E e^{-j2kt \sin\phi_0}) \frac{L_2(\lambda) U_4(\lambda_0)}{L_4(\lambda) U_2(\lambda_0)} \right\}, \quad (31)$$

where $\lambda_0 = \cos\phi_0$. These may now be substituted into (13) to obtain the field scattered by the loaded parallel-plate waveguide. This requires an evaluation of the resulting integrals as described next.

To compute the field diffracted by the geometry in Figure 2b, (31) is substituted in (13) and a steepest-descent-path approximation is performed for large $k\rho$. Noting that the pertinent saddle point is at $\alpha = \phi$ when $\phi < \pi$ and at $\alpha = 2\pi - \phi$ when $\phi > \pi$ we find that

$$E_z^s \sim S_{DD}(\phi, \phi_0) \frac{e^{-jk\rho}}{\sqrt{\rho}}$$

where $S_{DD}(\phi, \phi_o)$ is the direct diffraction coefficient given by

$$S_{DD}(\phi, \phi_o) = \frac{e^{-j\pi/4}}{2\sqrt{2\pi k}} \frac{\sqrt{1+\cos\phi}}{\sqrt{\kappa+\cos\phi}} \frac{\sqrt{2} \sin \frac{\phi}{2} \sqrt{\kappa-\cos\phi_o}}{\cos\phi + \cos\phi_o} \left(1 \right. \\ \left. e^{-j2kt \sin\phi} \right) \\ \left\{ (1 + R_E + T_E e^{-j2kt \sin\phi_o}) \frac{L_1(\cos\phi) U_3(\cos\phi_o)}{L_3(\cos\phi) U_1(\cos\phi_o)} \pm (1 + R_E - T_E e^{-j2kt \sin\phi_o}) \frac{L_2(\cos\phi) U_4(\cos\phi_o)}{L_4(\cos\phi) U_2(\cos\phi_o)} \right\}, \quad (32)$$

in which the upper sign holds for $0 < \phi < \pi$ and the lower for $\pi < \phi < 2\pi$.

For the computation of the field coupled into the waveguide ($x>0$), $k\rho$ cannot be assumed large. Therefore, one must employ a technique other than the steepest descent method for its evaluation. A standard procedure is to transform (13b) to the λ -plane giving

$$E_z^s = E_{z2}^s = \frac{1}{2\pi j} \int_{-\infty}^{\infty} \frac{\sqrt{\kappa-\lambda_o}}{\sqrt{\kappa+\lambda} (\lambda+\lambda_o)} \left\{ (1 + R_E + T_E e^{-j2kt \sin\phi_o}) \frac{U_3(\lambda_o)}{L_3(\lambda) U_1(\lambda) U_1(\lambda_o)} \right. \\ \left. \cos \left[k(y+t) \sqrt{\kappa^2 - \lambda^2} \right] + j (1 + R_E - T_E e^{-j2kt \sin\phi_o}) \frac{U_4(\lambda_o)}{L_4(\lambda) U_2(\lambda) U_2(\lambda_o)} \sin \left[k(y+t) \sqrt{\kappa^2 - \lambda^2} \right] \right\} \\ e^{-jkt \sqrt{\kappa^2 - \lambda^2}} e^{-jkx\lambda} d\lambda \quad (33)$$

Since $x>0$, the above integrals can be evaluated via the residue theorem after closing the path of integration by a semi-infinite contour in the lower half of the λ -plane. In doing this, it should be remarked, that the above integrand does not have a branch at $\lambda = \kappa$. Noting now that $U_{1,2}(\lambda)$ have zeros at

$$\lambda = \lambda_n = \sqrt{\kappa^2 - \left(\frac{n\pi}{2kt}\right)^2}, \quad (34)$$

we find

$$E_z^s = E_{z2}^s = \sum_{n=1,2,\dots}^{\infty} C_n \frac{\cos}{\sin} \left[\frac{n\pi}{2t}(y+t) \right] e^{-jkx \lambda_n} \quad (35)$$

where

$$C_{n_o}(\phi_o) = \begin{Bmatrix} -1 \\ -j \end{Bmatrix} e^{j \frac{n\pi}{2}} \left(\frac{2kt}{n\pi} \right) \frac{\sqrt{\kappa - \cos\phi_o} \sqrt{\kappa - \lambda_n}}{\cos\phi_o + \lambda_n} (1 + R_E \pm T_E e^{-j2kt \sin\phi_o})$$

$$\frac{U_3(\cos\phi_o)}{4}$$

$$\frac{U_1'(\lambda_n) U_1(\cos\phi_o) L_3(\lambda_n)}{2 \quad 2 \quad 4} \quad (36)$$

are the coupline coefficients. In the above, the subscripts o denote odd and even n , respectively, and

$$U_1'(\lambda_n) = \left. \frac{dU_1(\lambda)}{d\lambda} \right|_{\lambda = \lambda_n}$$

As a check, we note that when $\epsilon_T = \mu_T = 1$, (32) and (36) reduce to the known expressions given in [10]. In passing, we also note that if we were concerned with the modal fields in the region $x < 0$, we would also have to consider the residues of the poles corresponding to the zeros of $L_{3,4}(\cos\alpha)$. These are precisely the surface wave modes of a dielectric waveguide. Furthermore, any branch-cut contribution would also have to be included.

IV. Radiation and Reflection by a Waveguide Mode

This problem is illustrated by Figures 2d, 2e, and 2f. The modal field (see (34))

$$E_{z_0}^i = \frac{\cos}{\sin} \left[\frac{n\pi}{2t} (y + t) \right] e^{jkx \lambda_n} ,$$

$$H_{x_0}^i = + j \frac{Y}{\kappa} \left(\frac{n\pi}{2kt} \right) \frac{\sin}{\cos} \left[\frac{n\pi}{2t} (y + t) \right] e^{jkx \lambda_n}$$

is now assumed to be incident toward the waveguide mouth and present throughout the region $-\infty < x < \infty, 0 > y > -2t$.

Our solution for the radiated field and that reflected back into the waveguide will follow the same general steps employed in the plane wave incidence analysis. The sum of the radiated and reflected fields are now the scattered fields and since they are solely caused by the currents on the perfectly conducting half-plane they can again be represented by (13) - (14). In addition, all of the boundary conditions (B1) - (B6) stated earlier are still valid.

Their mathematical forms are now given by

$$(B1) \quad E_{z1}^s = E_{z2}^s \quad \text{over} \quad -\infty < x < \infty, \quad y = 0,$$

$$(B2) \quad E_{z2}^s = E_{z3}^s \quad \text{over} \quad -\infty < x < \infty, \quad y = -2t,$$

$$(B3) \quad H_{x1}^s = H_{x2}^s + H_x^i \quad \text{over} \quad x < 0, \quad y = 0,$$

$$(B4) \quad H_{x3}^s = H_{x2}^s + H_x^i \quad \text{over} \quad x < 0, \quad y = -2t,$$

$$(B5) \quad E_{z1}^s = 0 \quad \text{over} \quad x > 0, \quad y = 0,$$

$$(B6) \quad E_{z3}^s = 0 \quad \text{over} \quad x > 0, \quad y = -2t,$$

since E_z^i is already zero over the perfectly conducting half-planes.

Application of the boundary conditions (B1) - (B2) again result in the relations given

by (17). Thus the determination of $Q_{1,2}(\cos\alpha)$ is our only remaining task. To find these, we proceed with the application of boundary conditions (B3) and (B4), then add and subtract the resulting equations to obtain

$$\int_{-\infty}^{\infty} [Q_{1_e}(\lambda) + Q_{2_e}(\lambda)] \frac{\sqrt{\kappa^2 - \lambda^2}}{\sqrt{1 - \lambda^2}} L_3(\lambda) U_3(\lambda) e^{-jkx\lambda} d\lambda = \begin{cases} \frac{-j}{\mu_r + 1} \left(\frac{n\pi}{kt} \right) \sin\left(\frac{n\pi}{2}\right) e^{jkx\lambda_n} \\ 0 \end{cases} ; x < 0 , \quad (37)$$

$$\int_{-\infty}^{\infty} [Q_{1_e}(\lambda) - Q_{2_e}(\lambda)] \frac{\sqrt{\kappa^2 - \lambda^2}}{\sqrt{1 - \lambda^2}} L_4(\lambda) U_4(\lambda) e^{-jkx\lambda} d\lambda = \begin{cases} 0 \\ \frac{j}{\mu_r + 1} \left(\frac{n\pi}{kt} \right) \cos\left(\frac{n\pi}{2}\right) e^{jkx\lambda_n} \end{cases} ; x < 0 . \quad (38)$$

By enforcing boundary conditions (B5) - (B6) and again adding and subtracting the resulting equations, we also have that

$$\int_{-\infty}^{\infty} [Q_{1_e}(\lambda) + Q_{2_e}(\lambda)] \frac{1}{\sqrt{1 - \lambda^2}} L_1(\lambda) U_1(\lambda) e^{-jkx\lambda} d\lambda = 0 ; x > 0 , \quad (39)$$

$$\int_{-\infty}^{\infty} [Q_{1_e}(\lambda) - Q_{2_e}(\lambda)] \frac{1}{\sqrt{1 - \lambda^2}} L_2(\lambda) U_2(\lambda) e^{-jkx\lambda} d\lambda = 0 ; x > 0 . \quad (40)$$

Equations (37) with (39) and (38) with (40) form again a coupled set sufficient for

the solution of $Q_{1,2}(\lambda)$. In proceeding with this solution, we note that since (39) - (40) are

valid for $x > 0$, the path of integration may be closed by a semi-infinite contour in the lower half of the λ -plane, giving

$$[Q_{1_e}(\lambda) + Q_{2_e}(\lambda)] \frac{1}{\sqrt{1-\lambda^2}} L_1(\lambda) U_1(\lambda) = L_{A_e}(\lambda) \quad , \quad (41)$$

$$[Q_{1_e}(\lambda) - Q_{2_e}(\lambda)] \frac{1}{\sqrt{1-\lambda^2}} L_2(\lambda) U_2(\lambda) = L_{B_e}(\lambda) \quad (42)$$

where $L_A(\lambda)$ and $L_B(\lambda)$ are again unknown functions regular in the lower half λ -plane.

Similarly, because (37) - (38) apply to $x < 0$, we may close the path of integration with a semi-infinite contour in the upper half of the λ -plane resulting to

$$[Q_{1_e}(\lambda) + Q_{2_e}(\lambda)] \frac{\sqrt{\kappa^2 - \lambda^2}}{\sqrt{1-\lambda^2}} L_3(\lambda) U_3(\lambda) = \begin{cases} \frac{-n}{(\mu_r + 1) 2kt} \frac{\sin(\frac{n\pi}{2})}{\lambda + \lambda_n} \frac{U_{A_o}(\lambda)}{U_{A_o}(-\lambda_n)} \\ U_{A_e}(\lambda) E_A(\lambda) \end{cases} \quad (43)$$

$$[Q_{1_e}(\lambda) - Q_{2_e}(\lambda)] \frac{\sqrt{\kappa^2 - \lambda^2}}{\sqrt{1-\lambda^2}} L_4(\lambda) U_4(\lambda) = \begin{cases} U_{B_o}(\lambda) E_B(\lambda) \\ \frac{n}{(\mu_r + 1) 2kt} \frac{\cos(\frac{n\pi}{2})}{\lambda + \lambda_n} \frac{U_{B_e}(\lambda)}{U_{B_e}(-\lambda_n)} \end{cases} \quad (44)$$

where U_A, U_B are unknown functions regular in the upper half of the λ -plane and $E_{A,B}(\lambda)$ are unknown entire functions whose justification for the appearance of will soon become apparent. Substituting (41), (42) into (43), (44) respectively, and equating regions of regularity we find

$$U_{A_e}(\lambda) = U_A(\lambda) = \frac{U_3(\lambda) \sqrt{\kappa - \lambda}}{U_1(\lambda)}, \quad (45a)$$

$$U_{B_e}(\lambda) = U_B(\lambda) = \frac{U_4(\lambda) \sqrt{\kappa - \lambda}}{U_2(\lambda)}, \quad (45b)$$

$$L_{A_e}(\lambda) = \begin{cases} \frac{-\sin\left(\frac{n\pi}{2}\right)}{(\mu_r + 1)\pi} \frac{\sqrt{\kappa - \lambda_n}}{\sqrt{\kappa + \lambda} (\lambda + \lambda_n)} \frac{L_1(\lambda) L_1(\lambda_n)}{L_3(\lambda) L_3(\lambda_n)}, \\ \frac{L_1(\lambda)}{L_3(\lambda) \sqrt{\kappa + \lambda}} E_A(\lambda), \end{cases} \quad (45c)$$

$$L_{B_e}(\lambda) = \begin{cases} \frac{L_2(\lambda)}{L_4(\lambda) \sqrt{\kappa + \lambda}} E_B(\lambda), \\ \frac{\cos\left(\frac{n\pi}{2}\right)}{(\mu_r + 1)\pi} \frac{\sqrt{\kappa - \lambda_n}}{\sqrt{\kappa + \lambda} (\lambda + \lambda_n)} \frac{L_2(\lambda) L_2(\lambda_n)}{L_4(\lambda) L_4(\lambda_n)}. \end{cases} \quad (45d)$$

We may now use (17), (43), (44), and (45) to determine the spectra $P_{1,2}(\lambda)$ as

$$P_{1_e}(\lambda) = \frac{\sqrt{1 - \lambda^2} L_1(\lambda)}{2 \sqrt{\kappa + \lambda} L_3(\lambda)} E_A(\lambda) + \frac{\sin\left(\frac{n\pi}{2}\right)}{(\mu_r + 1) 2\pi} \frac{\sqrt{1 + \lambda}}{\sqrt{\kappa + \lambda}} \frac{\sqrt{1 - \lambda} \sqrt{\kappa - \lambda_n}}{\lambda + \lambda_n} \frac{L_1(\lambda) L_1(\lambda_n)}{L_3(\lambda) L_3(\lambda_n)}, \quad (46)$$

$$P_{2_o_e}(\lambda) = \mp \frac{\sqrt{1-\lambda^2} L_2(\lambda)}{2\sqrt{\kappa+\lambda} L_4(\lambda)} E_B(\lambda) - \frac{\sin(\frac{n\pi}{2})}{(\mu_r+1)2\pi} \frac{\sqrt{1+\lambda}}{\sqrt{\kappa+\lambda}} \frac{\sqrt{1-\lambda} \sqrt{\kappa-\lambda_n}}{\lambda+\lambda_n} \frac{L_2(\lambda) L_2(\lambda_n)}{L_3(\lambda) L_3(\lambda_n)}, \quad (47)$$

with the evaluation of $E_A(\lambda)$ and $E_B(\lambda)$ remaining. From a straight forward examination of the field behavior at the plate edges, it can be shown that [9] $P(\lambda) \sim \lambda^{-1/2}$ as $\text{Re}(\lambda) \rightarrow \infty$ and since $L_{1,2}(\lambda), L_{3,4}(\lambda) \rightarrow 1$ as $\text{Re}(\lambda) \rightarrow \infty$, one concludes that

$$E_A(\lambda) = E_B(\lambda) = 0 \quad (48)$$

Consequently, we find that

$$P_{1_o_e}(\lambda) = \pm P_{2_o_e}(\lambda) = \mp \frac{\sin(\frac{n\pi}{2})}{(\mu_r+1)2\pi} \frac{\sqrt{1+\lambda}}{\sqrt{\kappa+\lambda}} \frac{\sqrt{1-\lambda} \sqrt{\kappa-\lambda_n}}{\lambda+\lambda_n} \frac{L_2(\lambda) L_2(\lambda_n)}{L_3(\lambda) L_3(\lambda_n)}, \quad (49)$$

$$Q_{1_o_e}(\lambda) = \pm Q_{2_o_e}(\lambda) = \mp \frac{\sin(\frac{n\pi}{2})}{(\mu_r+1)2\pi} \frac{\sqrt{1+\lambda}}{\sqrt{\kappa+\lambda}} \frac{\sqrt{1-\lambda} \sqrt{\kappa-\lambda_n}}{\lambda+\lambda_n} \frac{L_2(\lambda_n)}{U_2(\lambda) L_3(\lambda) L_3(\lambda_n)}. \quad (50)$$

The radiated field is now found by substituting (49) into (13). After employing a steepest descent path evaluation of the resulting integrals for large $\kappa\rho$ we obtain

$$E_{z_0 e}^s = \begin{cases} E_{z1_0 e}^s; & 0 < \phi < \pi \\ E_{z3_0 e}^s; & \pi < \phi < 2\pi \end{cases} \sim \frac{e^{-jk\rho}}{\sqrt{\rho}} L_{n_0 e}(\phi) \quad (51)$$

where the launching coefficients $L_{n_0 e}(\phi)$ are given by

$$L_{n_0 e} = \begin{cases} A \sin\left(\frac{n\pi}{2}\right) \\ B \cos\left(\frac{n\pi}{2}\right) \end{cases} \frac{j e^{-j\pi/4}}{\sqrt{2\pi k} (\mu_r + 1)} \frac{\sqrt{1 + \cos\phi}}{\sqrt{\kappa + \cos\phi}} \frac{\sqrt{2} \sin\left(\frac{\phi}{2}\right) \sqrt{\kappa - \lambda_n}}{\cos\phi + \lambda_n} \frac{L_1(\cos\phi) L_1(\lambda_n)}{L_3(\cos\phi) L_3(\lambda_n)},$$

in which $A = -1$, $B = 1$ when $0 < \phi < \pi$ and $A = B = -e^{-j2kt \sin\phi}$ when $\pi < \phi < 2\pi$.

The field reflected back into the waveguide is E_{z2}^s in (13) and is evaluated by the same procedure employed for the coupled field. Specifically, we transform the integration path to the λ -plane and invoke Cauchy's theorem after closing the path of integration with a semi-infinite circle in the lower half of the λ -plane to obtain

$$E_{z_0 e}^s = E_{z2_0 e}^s = \sum_{m=1,2,\dots} R_{m_0 e} \frac{\cos\left[\frac{m\pi}{2t}(y+t)\right]}{\sin\left[\frac{m\pi}{2t}(y+t)\right]} e^{-jkx \lambda_m} \quad (53)$$

where

$$R_{m_0 e} = \frac{4kt \left\{ \begin{matrix} j \\ 1 \end{matrix} \right\} \sin\left(\frac{n\pi}{2}\right)}{m\pi (\mu_r + 1)} \frac{\sqrt{\kappa - \lambda_m} \sqrt{\kappa - \lambda_n}}{\lambda_n + \lambda_m} \frac{L_1(\lambda_n)}{U_1'(\lambda_m) L_3(\lambda_m) L_3(\lambda_n)} e^{-j \frac{m\pi}{2}}, \quad (54a)$$

$$R_{m_o n_e} = R_{m_e n_o} = 0 \quad (54b)$$

are the reflection coefficients.

Finally, the matrix elements Γ_{mn} due to reflection from a perfectly conducting slab are given for the E_z -polarization by

$$\Gamma_{mn} = \begin{cases} -1, & m = n, \\ 0, & m \neq n, \end{cases} \quad (55)$$

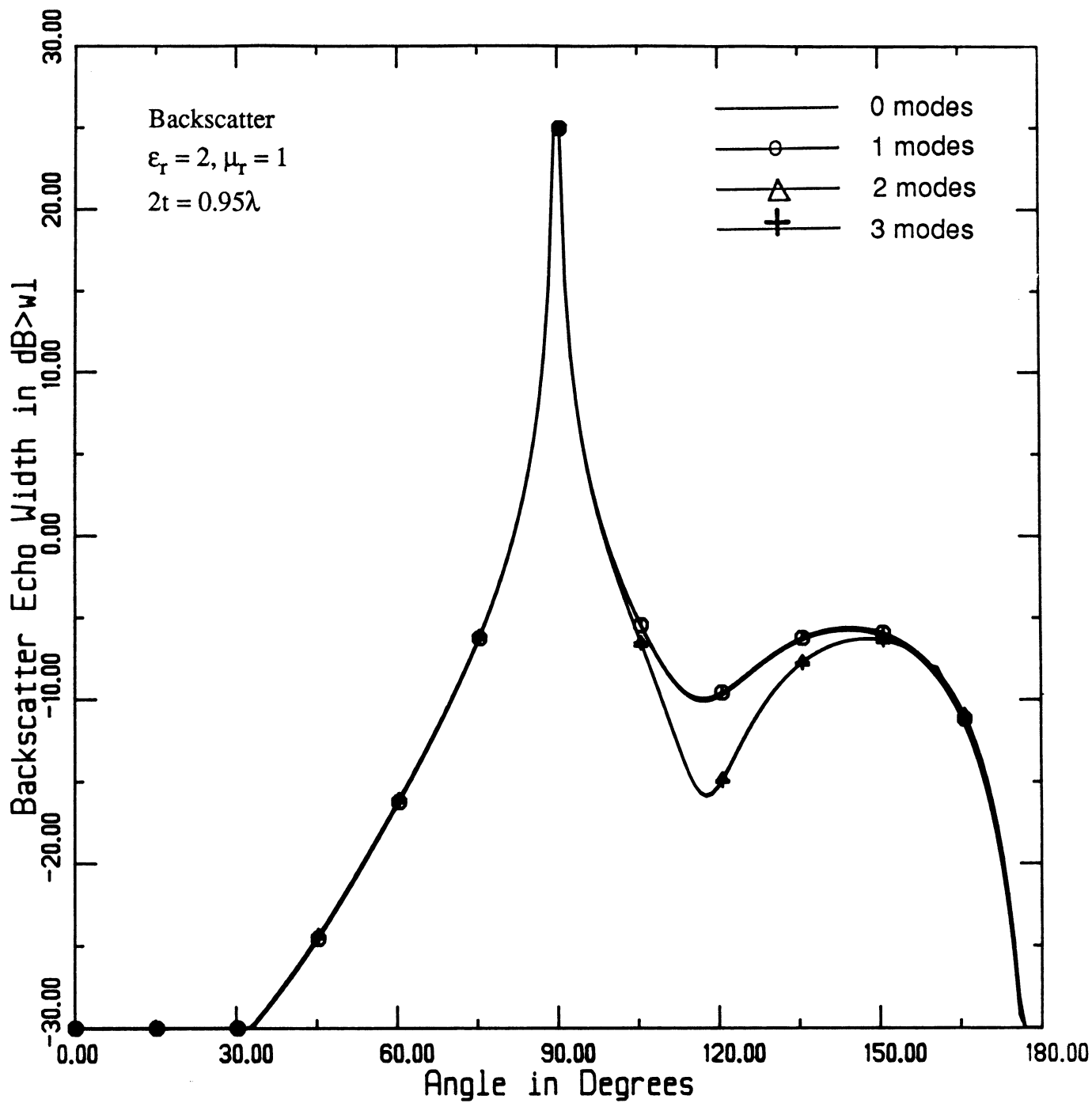
implying that $-\left[\Gamma_{mn}\right]$ is the identity matrix.

This completes the analysis required for the evaluation of the diffracted field E_z^s by the thick metallic-dielectric join shown in Figure 1. Below we present some numerical data which describe the scattering behavior of the metallic-dielectric join as function of thickness and the dielectric's constitutive parameters.

V. Numerical Results

Before proceeding with the computation of the diffracted field by the join as given in (1), it is essential to first determine the minimum number of modes required to achieve convergence of the infinite sum implied in (4). Such a test was performed in [10] for the thick perfectly conducting half-plane, equivalent to the dielectric-metallic join with $\epsilon_r = \mu_r = 1$. However, the conclusions in [10] are incorrect due to a programming error in the computation of the higher order modal fields and thus one cannot draw expectation from these results.

The convergence behavior of the backscattered field is presented in Figure 6 for a dielectric-metallic join .95-wavelengths-thick and for the three sets of material parameters $(\epsilon_r = 2-j.0, \mu_r = 1-j.0)$, $(\epsilon_r = 5-j.5, \mu_r = 1.5-j.1)$, and $(\epsilon_r = 7.4-j1.1, \mu_r = 1.4-j.672)$. In each case,



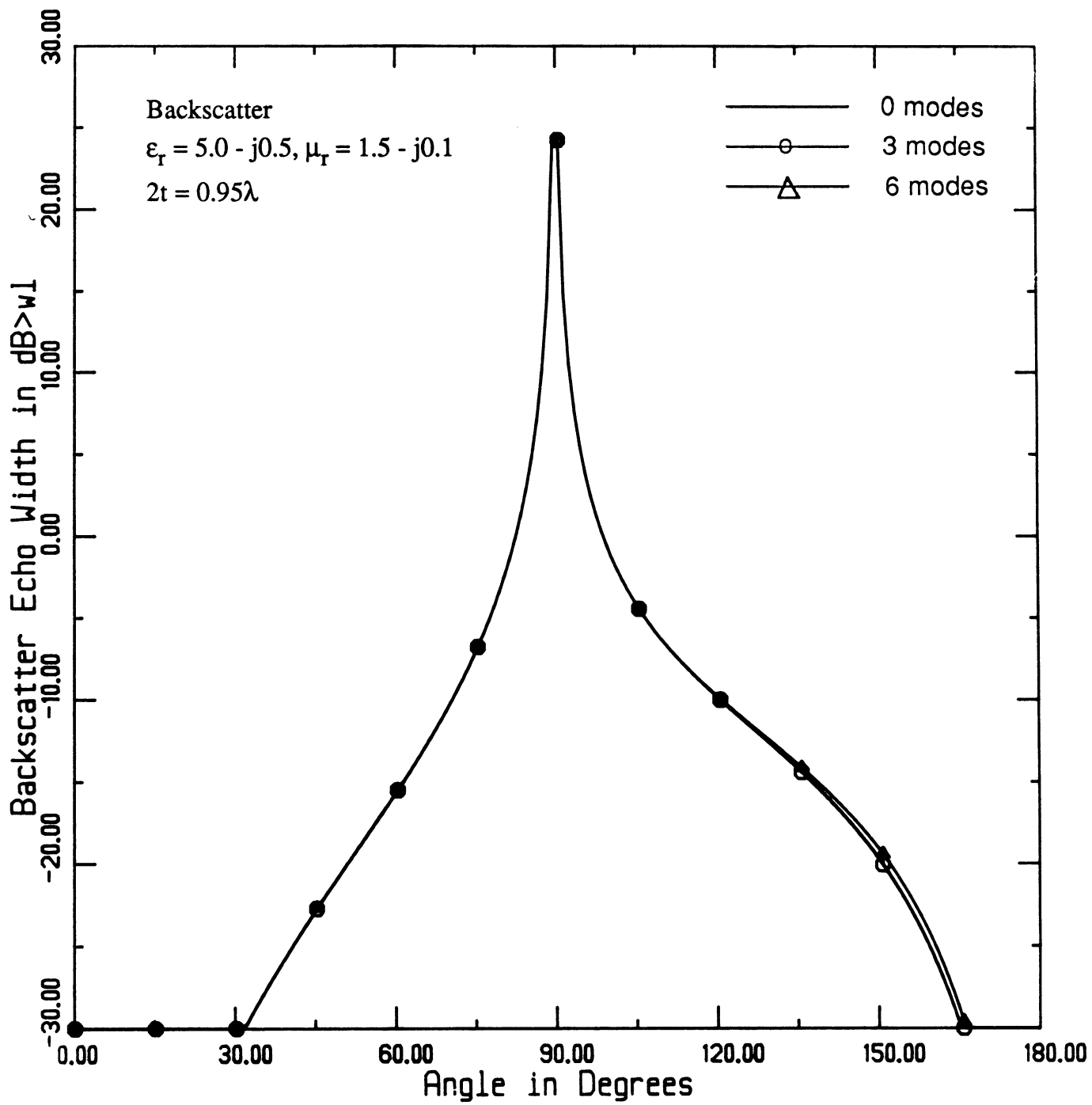
(a)

Fig. 6. Convergence test of the solution given in equation (1).

(a) $2t = 0.95\lambda, \epsilon_T = 2, \mu_T = 1.$

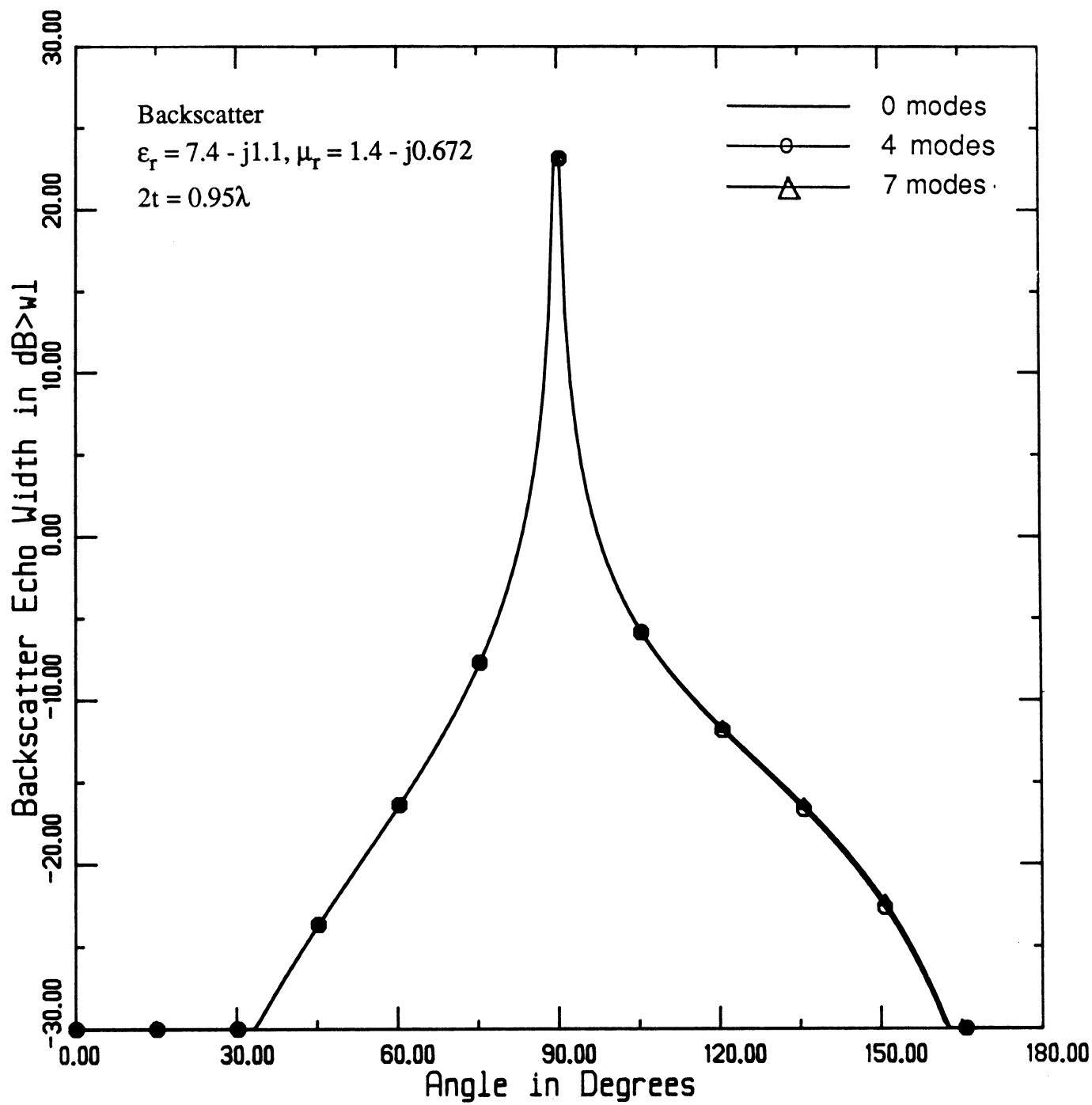
(b) $2t = 0.95\lambda, \epsilon_T = 5 - j0.5, \mu_T = 1.5 - j0.1.$

(c) $2t = 0.95\lambda, \epsilon_T = 7.4 - j1.1, \mu_T = 1.4 - j0.672.$



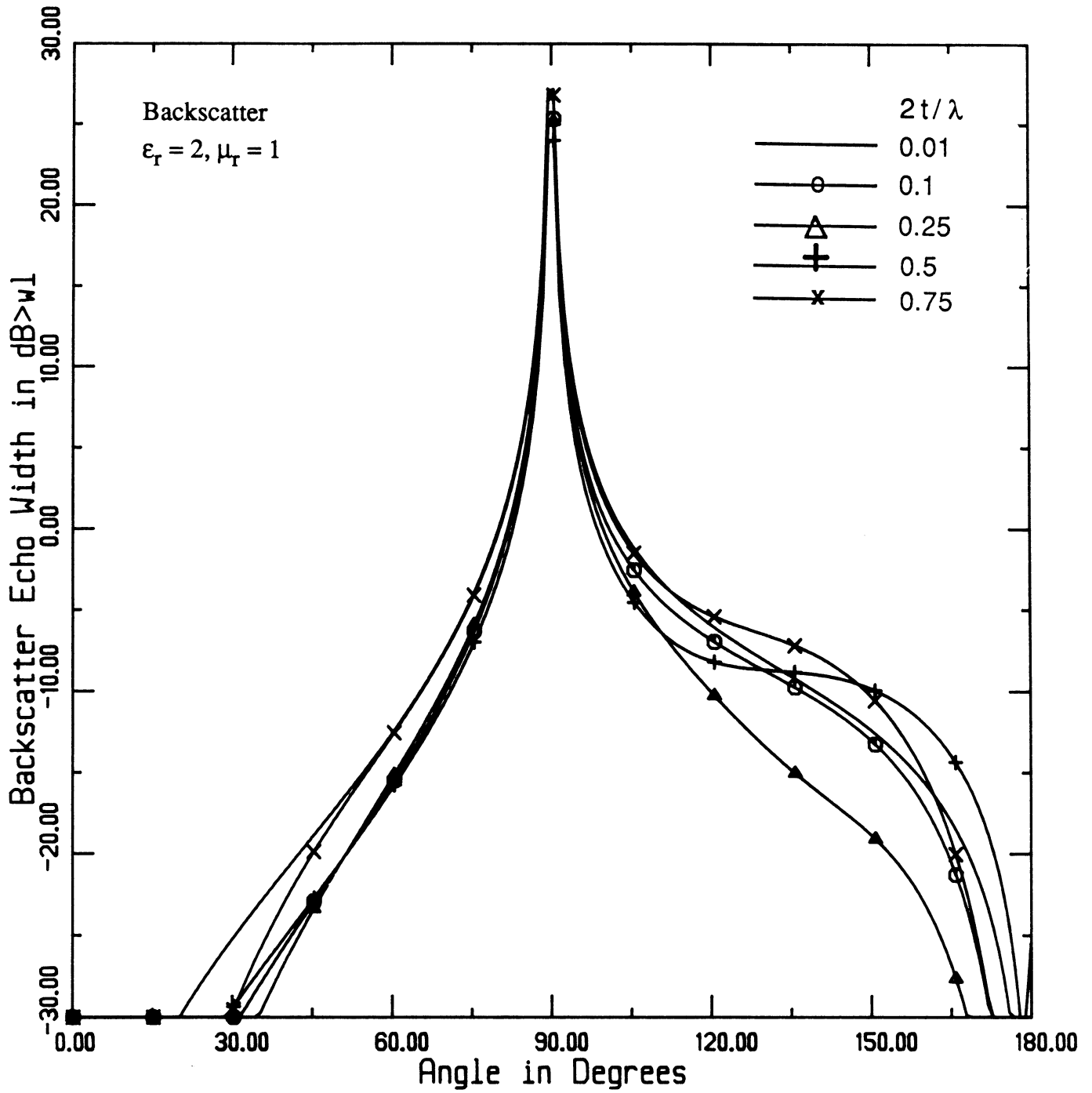
(b)

Fig. 6. Cont.



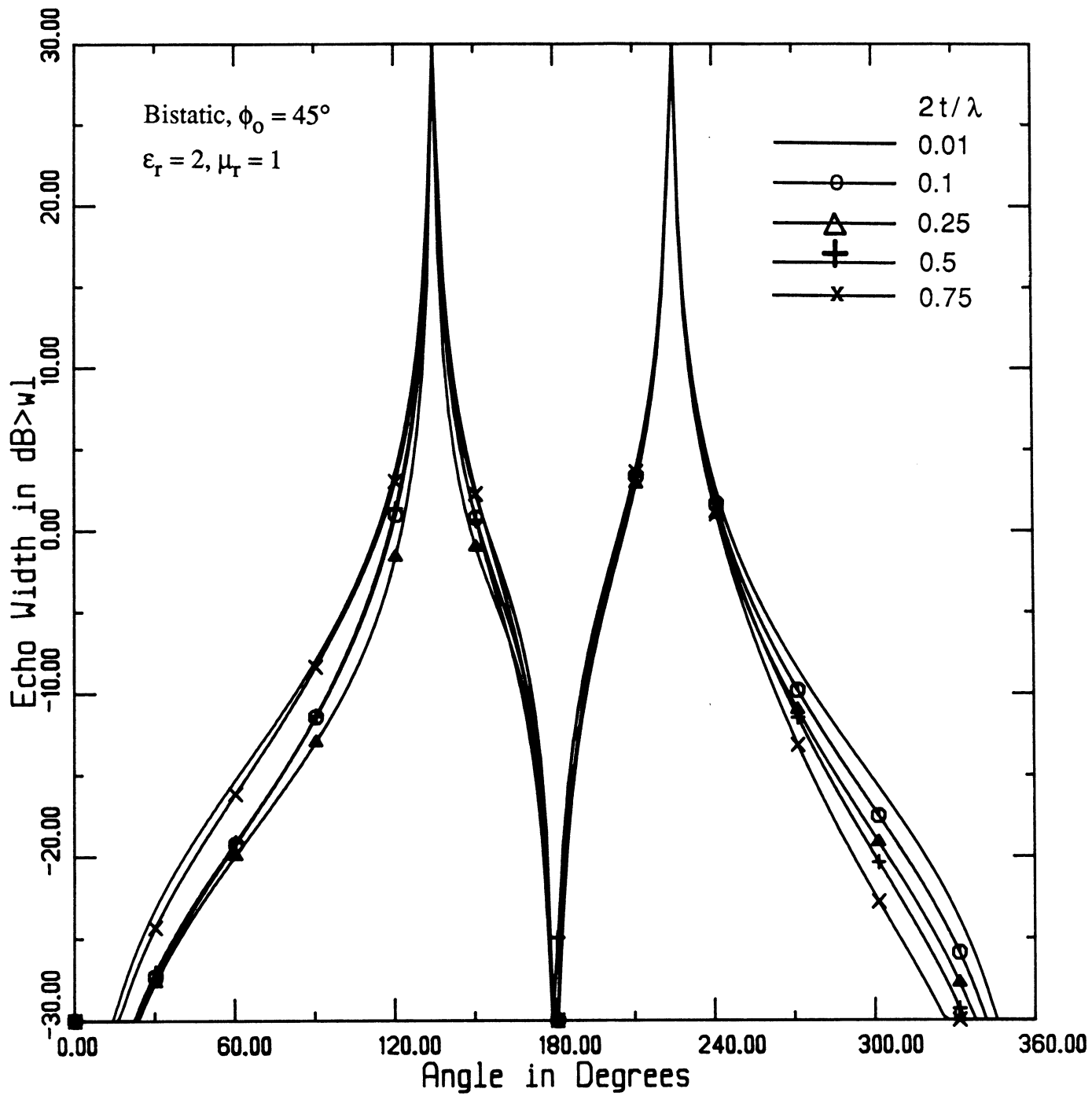
(c)

Fig. 6. Cont



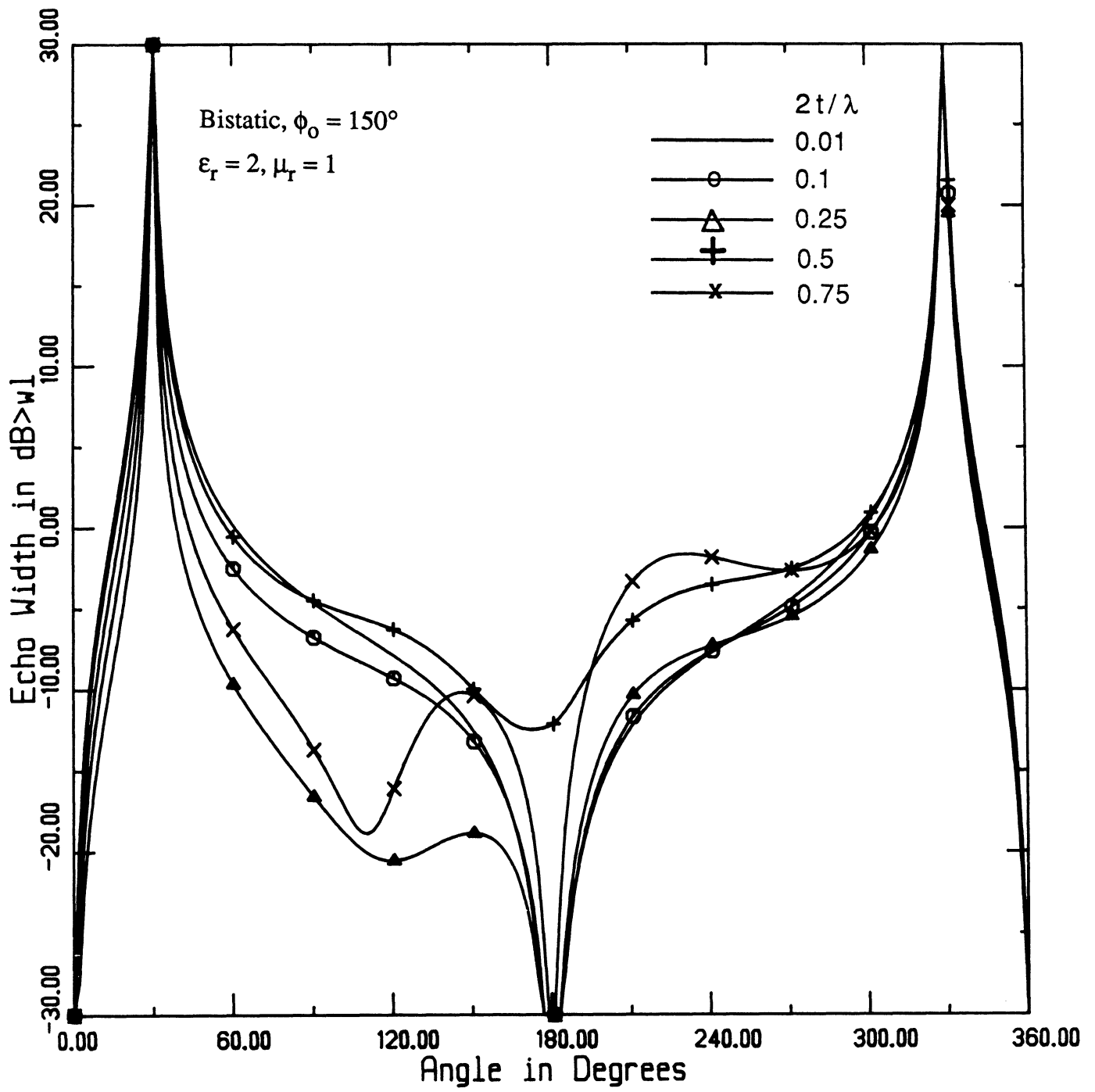
(a)

Fig. 7. E_z -polarization calculated echowidth family curves for $2t = 0.01, 0.1, 0.25, 0.5$ and 0.75 wavelengths. The constitutive parameters of the dielectric are $\epsilon_T = 2, \mu_T = 1$.
 (a) Backscatter case. (b) Bistatic with $\phi_0 = 45^\circ$. (c) Bistatic with $\phi_0 = 150^\circ$.



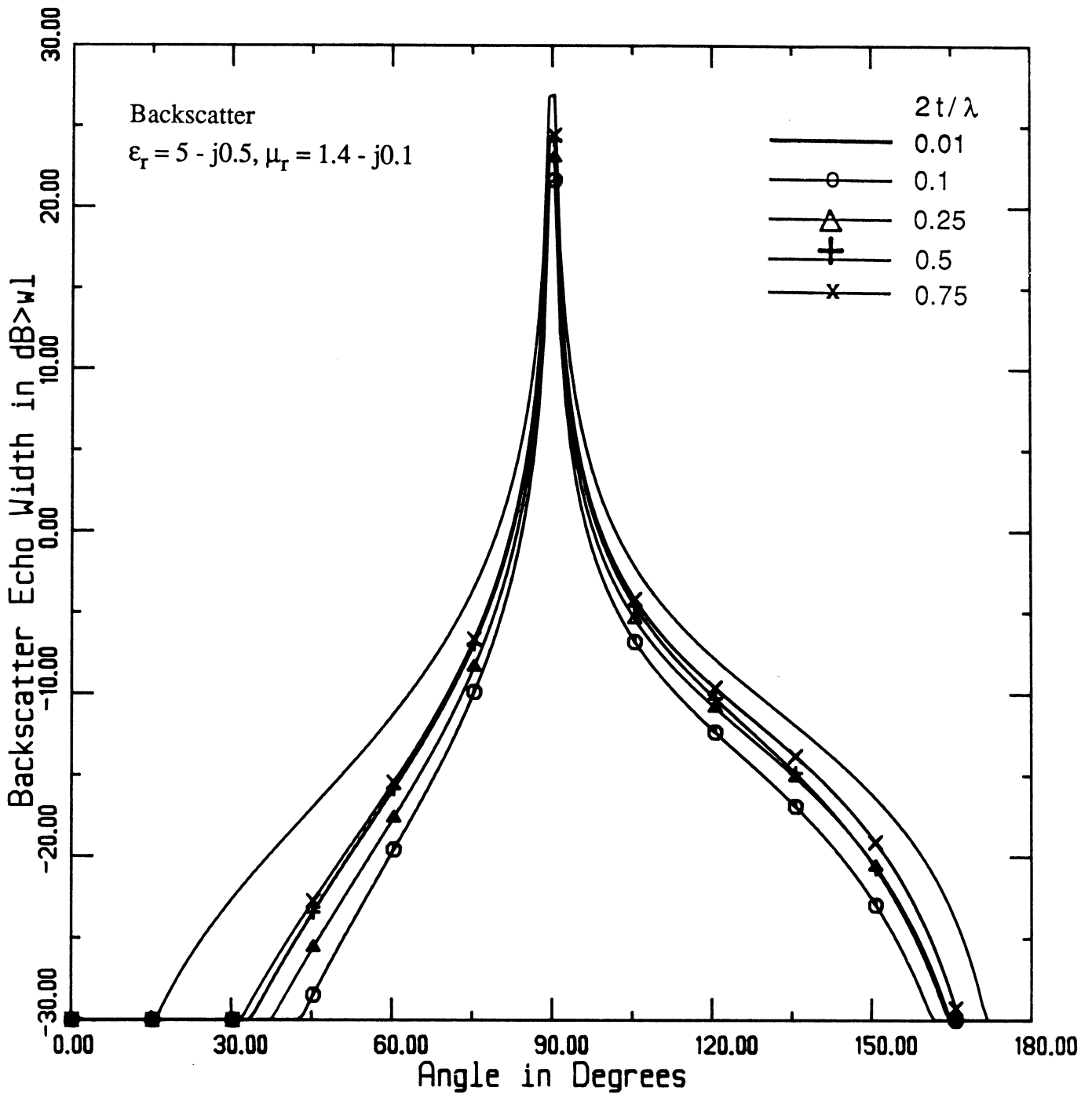
(b)

Fig. 7. Cont.



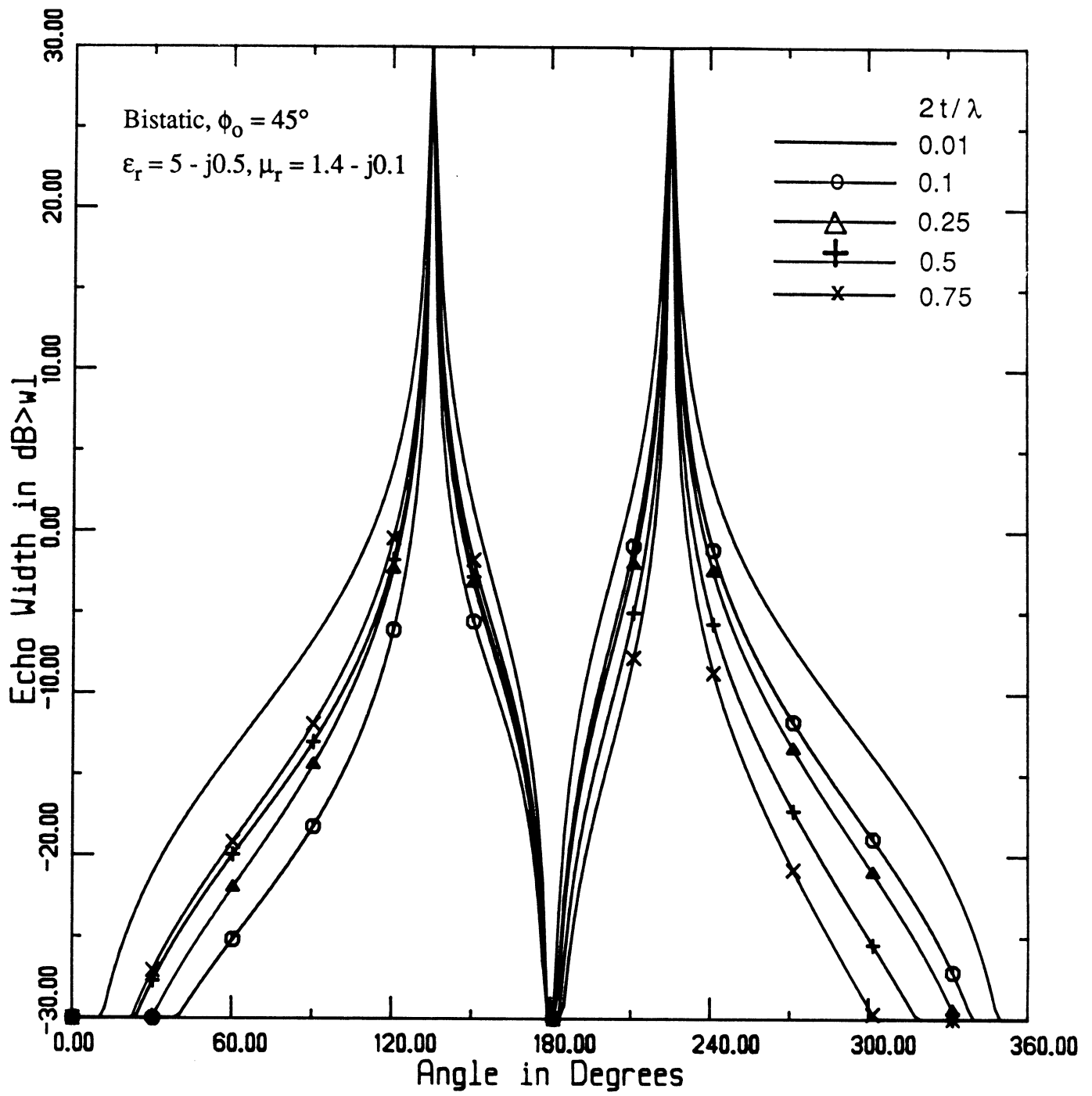
(c)

Fig. 7. Cont.



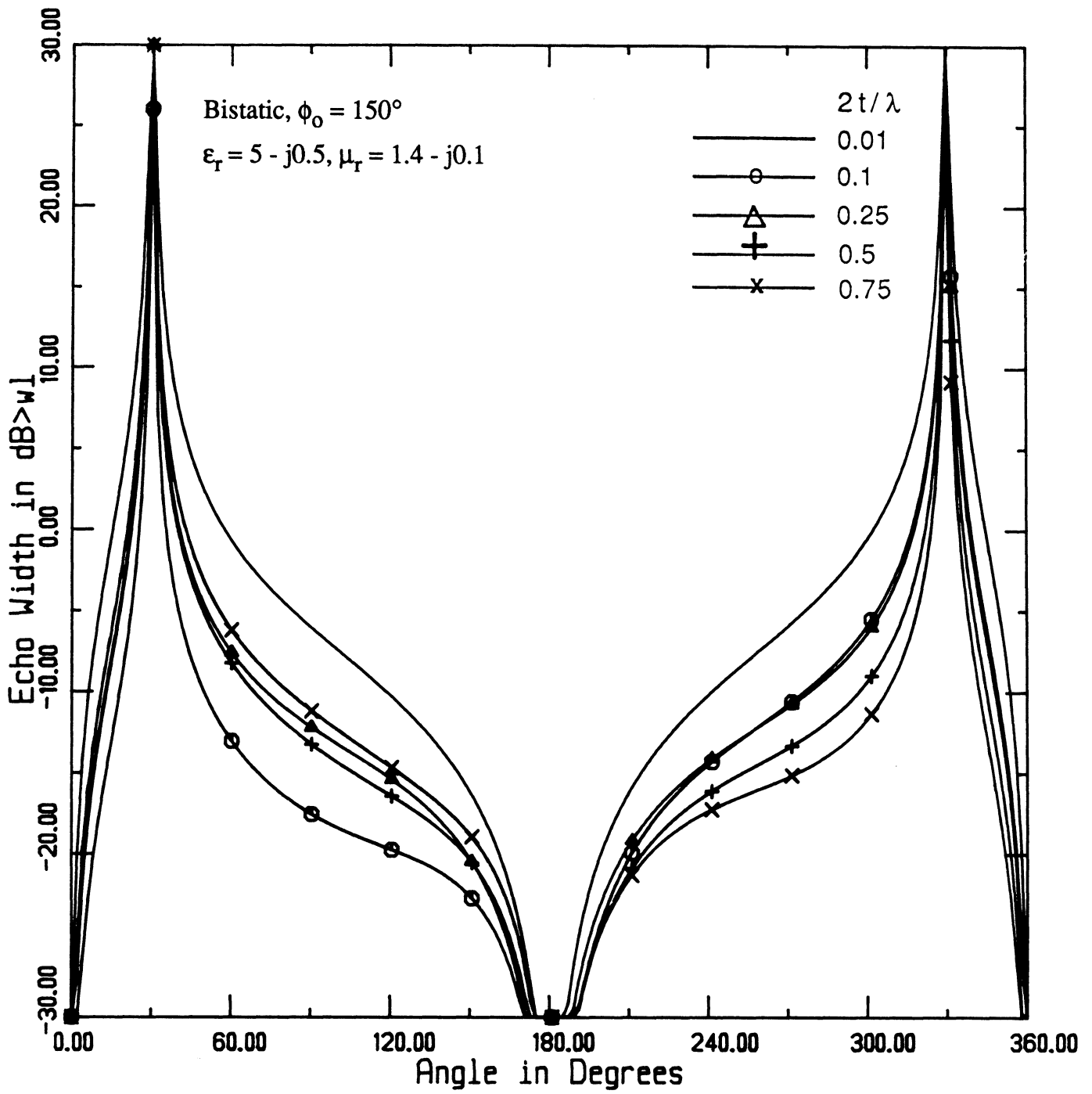
(a)

Fig. 8. E_z -polarization calculated echowidth family curves for $2t = 0.01, 0.1, 0.25, 0.5$ and 0.75 wavelengths. The constitutive parameters of the dielectric are $\epsilon_r = 5 - j0.5$, $\mu_r = 1.4 - j0.1$. (a) Backscatter case. (b) Bistatic, $\phi_0 = 45^\circ$. (c) Bistatic, $\phi_0 = 150^\circ$.



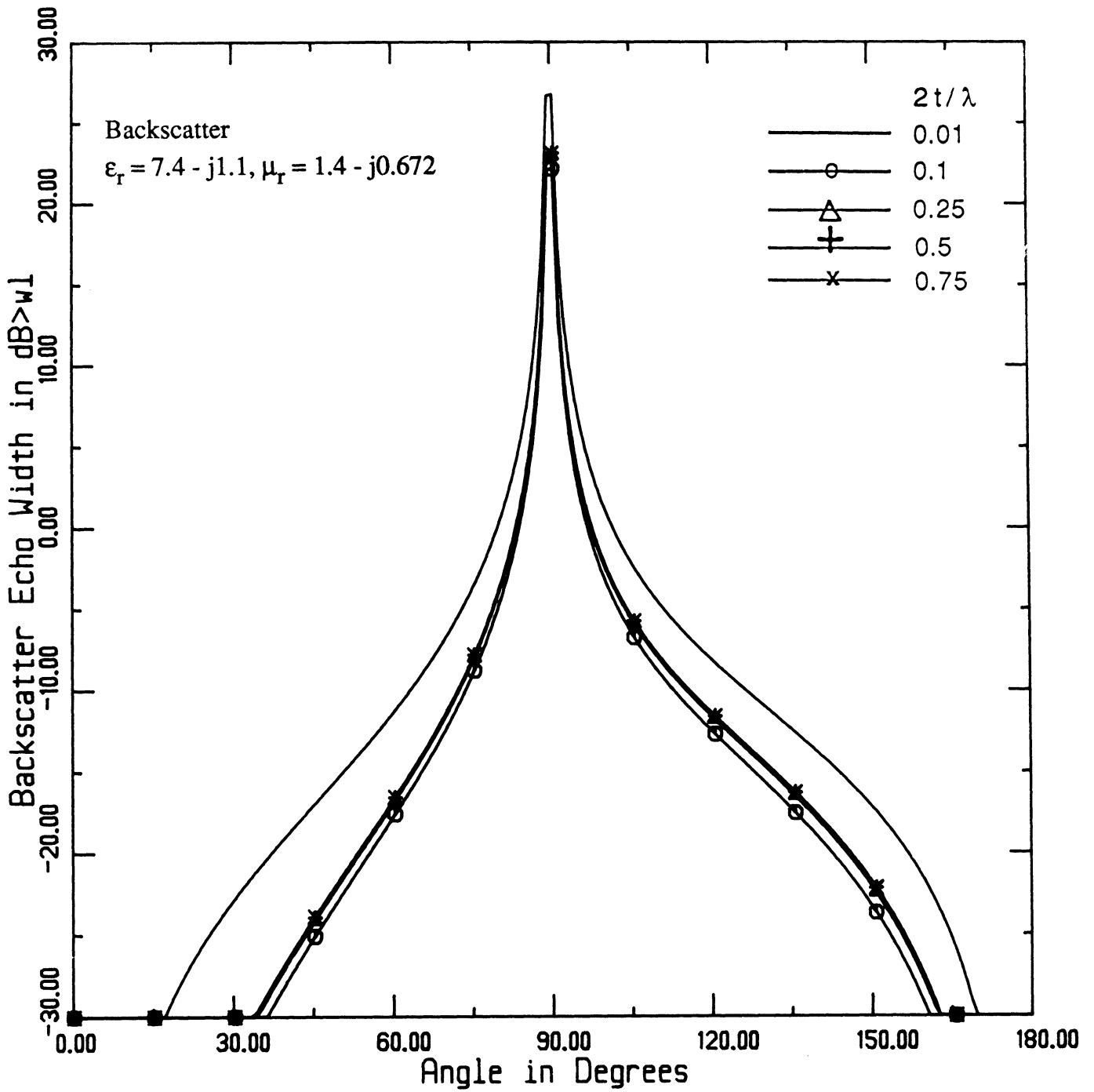
(b)

Fig. 8. Cont.



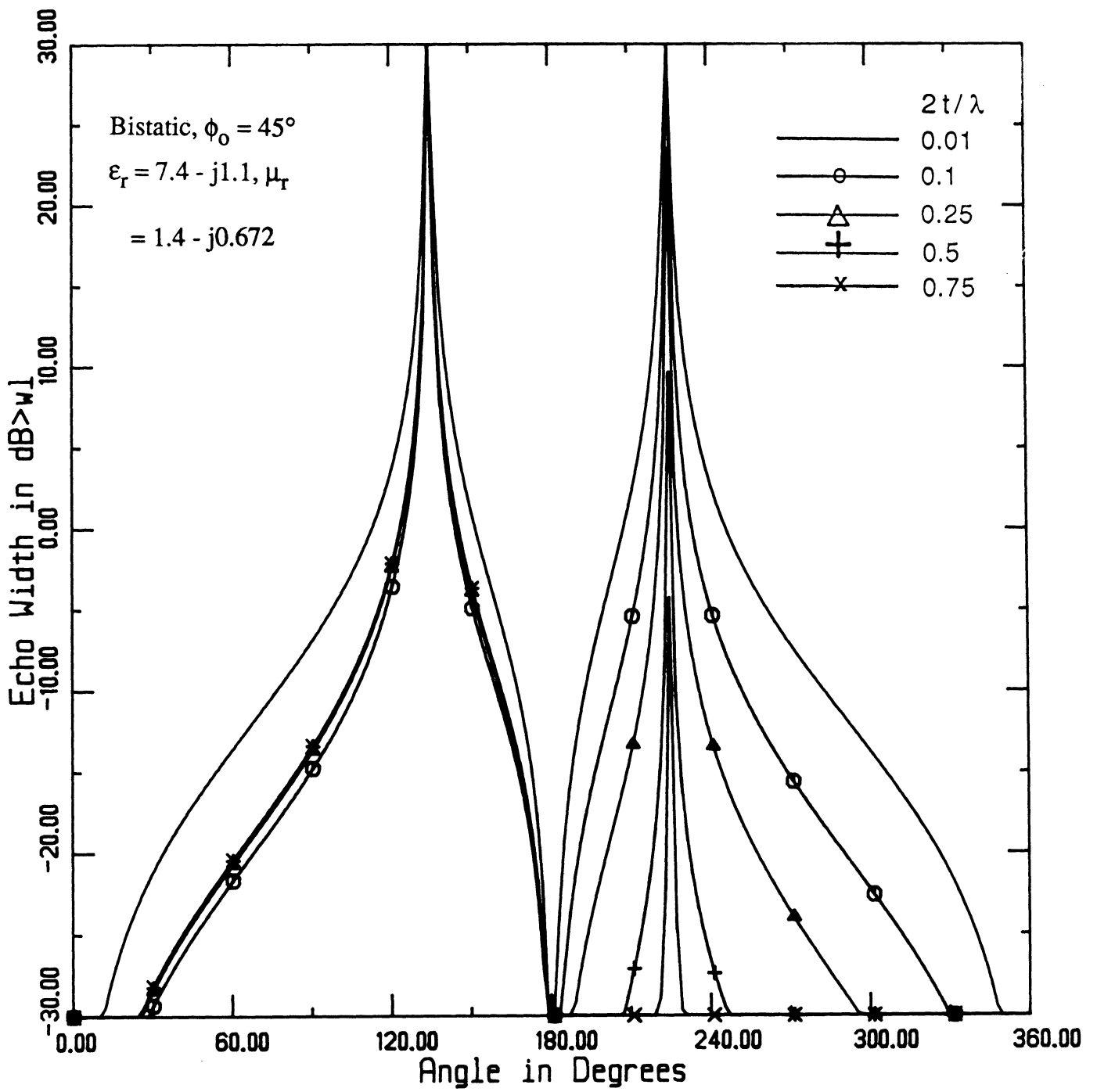
(c)

Fig. 8. Cont.



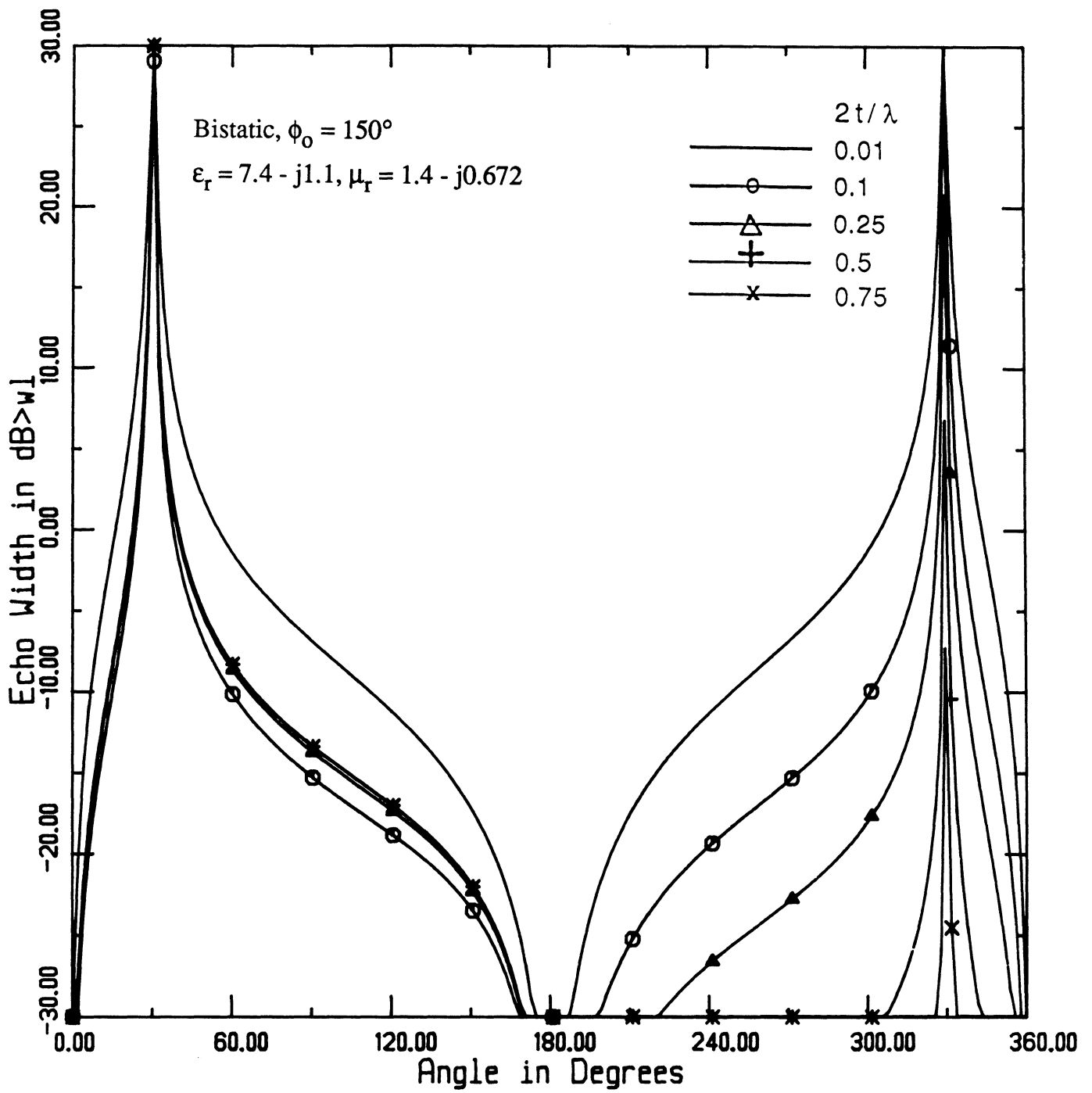
(a)

Fig. 9. E_z -polarization calculated echowidth family curves for $2t = 0.01, 0.1, 0.25, 0.5$ and 0.75 wavelengths. The constitutive parameters of the dielectric are $\epsilon_r = 7.4 - j1.1$ and $\mu_r = 1.4 - j.672$. (a) Backscatter case. (b) Bistatic, $\phi_0 = 45^\circ$. (c) Bistatic, $\phi_0 = 150^\circ$.



(b)

Fig. 9. Cont.



(c)

Fig. 9. Cont.

it is seen that the scattered field is well-converged with the inclusion of modes up to the first evanescent one. It is also apparent that an increase in material loss decreases the significance of the modes, allowing the converged field to be more closely approximated by the direct diffracted field.

Having established the convergence of the solution (1), we may now proceed with the computation of the field scattered by the dielectric-metallic join given in Figure 1. Backscattering and bistatic echo width curves are given in Figures 7 - 9 for dielectric-metallic joins of thickness varying from $2t/\lambda = .01$ to $2t/\lambda = .75$. Each figure includes backscatter and bistatic curves corresponding to one of the material parameter sets chosen above. Unfortunately, comparison with alternate solutions is not possible since to the author's knowledge neither experimental nor alternative analytical results are presently available.

VI. Summary

The dual integration approach has been used along with the generalized scattering matrix formulation to obtain the field scattered from a dielectric-metallic join for an E_z -polarized incident plane wave. This was accomplished by first considering the diffraction from the loaded parallel-plate waveguide with a recessed stub (Figure 2a) and subsequently restoring the distance between the stub and the waveguide mouth to zero. The solution to the recessed-stub geometry was formulated via the GSMF, requiring in turn solution of the five subproblems illustrated in Figures 2b-2f. We initially considered the subproblems of the direct diffraction and mode coupling of an incident plane wave on the loaded parallel plate waveguide. The problems of radiation and reflection due to waveguide mode incident upon the waveguide mouth was considered next. In both cases the scattered field was expressed by a suitable angular spectrum representation involving unknown spectral functions. These were then determined via application of the necessary boundary conditions and explicit expressions for the scattered fields were subsequently obtained by employing an asymptotic or residue

series evaluation of the pertinent integrals. Implicit in this analysis is the Wiener-Hopf factorization of several functions and in some cases this was accomplished via numerical means using a new technique described in Appendix B.

At the end of the report, the convergence behavior of the scattered field with respect to the number of included modes was examined for three different material compositions and it was found that inclusion of modes up to the first evanescent one provided a well-converged result. It was also seen that an increase in material loss de-emphasized the modal contribution to the diffracted field. Finally, families of backscattering and bistatic echowidth curves for join thicknesses ranging from $0.01\lambda < 2t < .75\lambda$ were presented for various sets of ϵ_T, μ_T .

REFERENCES

1. C.P. Bates and R. Mittra, "Waveguide Excitation of Dielectric and Plasma Slabs," *Radio Science*, Vol. 3, No. 3, pp. 251-266, March 1968.
2. K. Uchida and K. Aoki, "Radiation From and Surface Wave Excitation by an Open-Ended Dielectric-Loaded Parallel-Plate Waveguide," *The Transactions of the IECE of Japan*, Vol. E-67, No. 4, pp. 218-224, April 1984.
3. T.T. Fong, "Radiation From an Open-Ended Waveguide With Extended Dielectric Loading," *Radio Science*, Vol. 7, No. 10, pp. 965-972, October 1972.
4. K. Aoki and K. Uchida, "Scattering of a Plane Electromagnetic Wave by Two Semi-Infinite Dielectric Slabs," *The Transactions of the IECE of Japan*, Vol. 62-B, No. 12, pp. 1132-1139, 1979.
5. J.R. Pace and R. Mittra, "Generalized Scattering Matrix Analysis of Waveguide Discontinuity Problems," *Proc. Symp. Quasi-Optics*, Vol. 14, Brooklyn, N.Y., Polytechnic Inst. of Brooklyn Press, pp. 177-197, 1964.
6. P.C. Clemmow, "A Method for the Exact Solution of a Class of Two-Dimensional Diffraction Problems," *Proc. Roy Soc. A.*, Vol. 205, pp. 286-308, 1951.
7. S.W. Lee and R. Mittra, "Diffraction by Thick Conducting Half-Plane and a Dielectric-Loaded Waveguide," *IEEE Transactions on Antennas and Propagation*, Vol. AP-16, No. 4, pp. 454-461, July 1968.
8. B. Noble, Methods Based on the Wiener-Hopf Technique, Chapter 1, Pergamon, 1958.
9. R. Mittra and S.W. Lee, Analytical Techniques in the Theory of Guided Waves, pp. 4-11, MacMillan, 1971.
10. J.L. Volakis and M.A. Ricoy, "Diffraction by a Thick Conducting Half-Plane," *IEEE Transactions on Antennas and Propagation*, Vol. AP-35, pp. 62-72, January 1987.
11. R.D. Coblin, "Scattering of an Electromagnetic Plane Wave From a Perfectly Electrically Conducting Half-Plane in the Proximity of Planar Media Discontinuities," Ph.D. dissertation, Univ. of Mississippi, 1983, pp. 122-129.

Appendix A

Expressions for the Split Functions $L_{1,2}(\lambda)$ and $U_{1,2}(\lambda)$

The split functions $U_{1,2}$ and $L_{1,2}$ arise in the factorization of the functions

$(1 \pm e^{-j2kt\sqrt{\kappa^2 - \lambda^2}})$ as follows:

$$1 \pm e^{-j2kt\sqrt{\kappa^2 - \lambda^2}} = U_{\frac{1}{2}}(\lambda) L_{\frac{1}{2}}(\lambda) . \quad (A1)$$

The U functions are free of branch cuts, poles and zeros (i.e., regular) in the upper half of the λ -plane shown in Fig. 5. Similarly the L functions are regular in the lower half of the λ -plane.

These functions may be derived using the procedure given by Noble [8]. The appropriate expressions for the $e^{j\omega t}$ convention employed in this paper are

$$U_1(\lambda) = L_1(-\lambda) = \sqrt{2} \exp[-T(\lambda) - X_1(\lambda)] \prod_{n=1,3,5}^{\infty} \left(\frac{-j2kt}{n\pi} \right) (\lambda - \lambda_n) \exp(j2kt\lambda/n\pi) , \quad (A2)$$

$$U_2(\lambda) = L_2(-\lambda) = e^{j\pi/4} \sqrt{2kt\sqrt{\kappa - \lambda}} \exp[-T(\lambda) - X_2(\lambda)] \prod_{n=2,4,6}^{\infty} \left(\frac{-j2kt}{n\pi} \right) (\lambda - \lambda_n) \exp(j2kt\lambda/n\pi) , \quad (A3)$$

where

$$T(\lambda) = -jkt\sqrt{\kappa^2 - \lambda^2} \left[1 - \frac{\cos^{-1}(\lambda/\kappa)}{\pi} \right] , \quad (A4)$$

$$X_2(\lambda) = \frac{j\lambda kt}{\pi} \left[0.4228 + \ln \left(\frac{\pi}{k't} \right) + \ln 2 \right] + \frac{kt\lambda}{2} , \quad (A5)$$

and

$$\lambda_n = \sqrt{\kappa^2 - \left(\frac{n\pi}{2kt}\right)^2} . \quad (\text{A6})$$

The branch of the above logarithm is defined such that $-\pi \leq \text{Im}(\ln) < \pi$, while all other branches in the above expression are explicitly defined in Figures 3, 4, and 5.

Appendix B

An Efficient Numerical Wiener-Hopf Factorization Method

A crucial and major step in obtaining a solution to a Wiener-Hopf equation is the factorization/splitting of an even function $F(\alpha)$ into a product of two functions such that

$$F(\alpha) = L(\alpha) U(\alpha) \tag{B1}$$

where $\alpha = \sigma + j\tau$. In the above, $U(\alpha)$ is free of zeros, poles and branch cuts (i.e., regular) in the upper half of the α -plane ($\tau > \tau_-$) shown in Figure B1, while $L(\alpha)$ is regular in the lower half of the α -plane ($\tau < \tau_+$), where $\tau_- < \tau_+$. To accomplish the factorization (B1) we must generally assume that $F(\alpha)$ is regular within the strip $\tau_- < \tau < \tau_+$, where τ_{\pm} are allowed to approach vanishing values. If we further demand that $F(\alpha) \rightarrow 1$ uniformly as $|\sigma| \rightarrow \infty$ within the strip, then $U(\alpha)$ and $L(\alpha)$ are formally given by [9]

$$U(\alpha) = L(-\alpha) = \exp[H(\alpha)] , \text{Im}(\alpha) > 0 \tag{B2}$$

where

$$H(\alpha) = \frac{1}{2\pi j} \int_{C_1} \frac{\ln[F(\beta)]}{\beta - \alpha} d\beta \tag{B3}$$

with C_1 as shown in Figure B1. Note, however, that this last condition on $F(\alpha)$ does not necessarily restrict its form since any $F(\alpha)$ can be modified as such in a recoverable manner. Additionally, due to the even property of $F(\alpha)$, we may set $\tau_- = -\tau_+$ implying that the contour

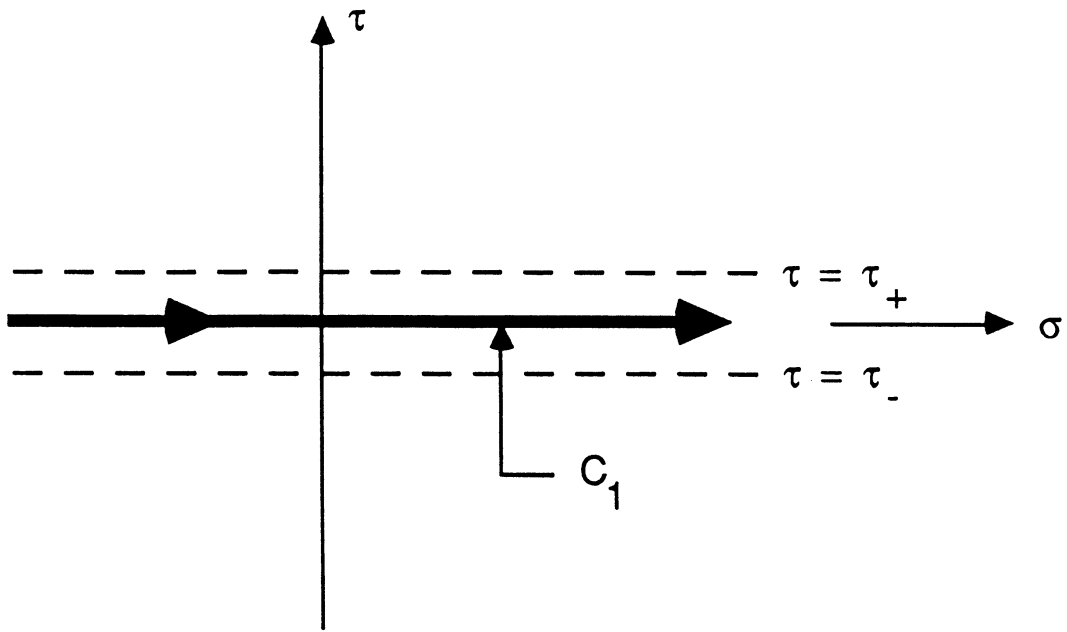


Figure B1. Illustration of C_1 contour.

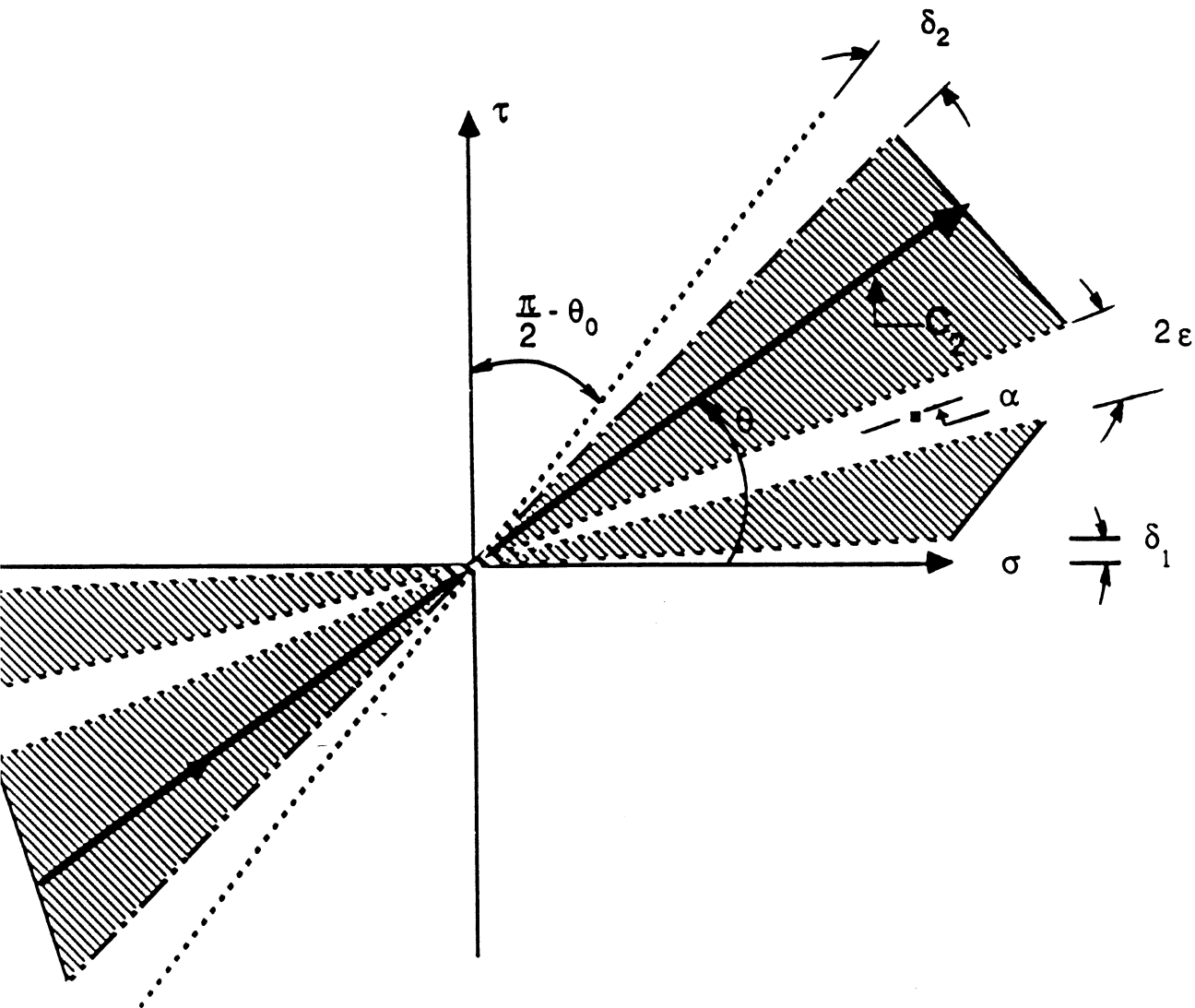


Figure B2. Illustration of the C_2 contour with the permitted values of θ .

C_1 ($\tau = 0$) remains within the strip $|\tau| < \tau_+$ as τ_{\pm} become arbitrarily small.

Despite its general applicability, (B2) contains several barriers to its direct numerical implementation. In addition to displaying infinite limits of integration, the contour integral possesses an integrand which may become singular depending on the contour's location. Further, care must be exercised to insure that a proper branch of the logarithm is taken so that $\ln[F(\beta)]$ is continuous on C_1 . Under certain circumstances, however, these problems can be largely alleviated via appropriate modification of (B2).

To this end, suppose that in addition to being regular in the strip $|\tau| < \tau_+$, $F(\beta)$ is also regular in the angular sector $\{\beta(t) = te^{j\theta}; 0 < \theta < \theta_0, 0 < t < \infty\}$ for some θ_0 and $F(\beta(t)) \rightarrow 1$ uniformly as $t \rightarrow \infty$ throughout the above sector. Since $F(\beta)$ is even, this also implies it will have the same properties in the additional angular sector $\{\beta(t) = te^{j\theta}; \pi < \theta < \pi + \theta_0, 0 < t < \infty\}$. Further, it should be noted that in general most functions requiring factorization in diffraction theory are of this type and, therefore, this is not a significant restriction on $F(\alpha)$. With the above provisions on the regularity of $F(\beta)$, it follows that C_1 can be rotated counter-clockwise about the origin by an angle θ ($0 < \theta < \theta_0$) to contour C_2 , as shown in Figure B2. $H(\alpha)$ is thus modified a

$$H(\alpha) = h(\theta - \theta_{\alpha}) \ln[F(\alpha)] + \frac{1}{2\pi j} \int_{C_2} \frac{\ln[F(\beta)]}{\beta - \alpha} d\beta, \quad (B3)$$

where

$$h(\theta - \theta_{\alpha}) \equiv \begin{cases} 0 & \text{for } \theta < \theta_{\alpha} , \\ 1 & \text{for } \theta > \theta_{\alpha} , \end{cases} \quad (B4)$$

and

$$\theta_\alpha = \arctan \left[\frac{\text{Im}(\alpha)}{\text{Re}(\alpha)} \right]. \quad (\text{B5})$$

Addressing the singularities associated with the integrand of (B3), it is clear that the numerator becomes infinite when $\beta = \beta_n$, where $\beta_n, n = 1, 2, \dots, N$ are the N zeros of $F(\beta)$. By virtue of the stipulated regularity of $F(\beta)$ in the angular sectors defined above, β_n are, however, precluded from lying upon the contour C_2 . Nevertheless, as θ approaches 0 or θ_0 , it is possible for any of the β_n to become arbitrarily close to C_2 (for $\theta \rightarrow 0$, this is true if τ_\pm tend to zero, which is often the case). Fortunately, the resulting singularity is logarithmic, implying that it need be removed only a small distance from the contour C_2 to substantially reduce the singularity of the integrand. The obvious solution, therefore, is to restrict the permissible angular variation to $\delta_1 < \theta < \theta_0 - \delta_2$, where $\delta_{1,2}$ are small angles which may be determined empirically. This scheme will work provided β_n are not in the vicinity of the origin, which prevents the contour in being distanced from the pertinent β_n via a simple rotation.

In contrast to the numerator which may display a multitude of singularities, the denominator contains a single zero at $\beta = \alpha$. Recall that the only condition on α is that $\text{Im}(\alpha) > 0$, admitting the possibility of α lying close to or upon C_2 . The simplest method to prevent this is to again impose restrictions on θ , so that $\theta \notin [\theta_{\alpha+\varepsilon}, \theta_{\alpha-\varepsilon}]$, where $\theta_\alpha = \arctan \left[\frac{\text{Im}(\alpha)}{\text{Re}(\alpha)} \right]$ and ε is a small angle to be determined empirically. However, the involved singularity is of higher-order than the one previously encountered, implying that $\varepsilon \gg \delta$. This greatly restricts the permitted range of θ if $0 < \theta_\alpha < \theta_0$, and is undesirable since the quantity $\ln[F(\beta)]$ may exhibit different rates of convergence as $\beta(t) \rightarrow \infty$ among the admissible θ . One would therefore prefer to

choose an optimum path C_2 from the standpoint of numerical accuracy. Hence, it is of interest to reduce the restricted range $[\theta_\alpha + \varepsilon, \theta_\alpha - \varepsilon]$ so that the likelihood of this range superimposing itself upon a region of optimum convergence is minimized. An appropriate modification to (B3) for accomplishing this is considered next.

The integral in (B3) is obviously not convenient for numerical implementation and it is therefore necessary to rewrite it for that purpose. By introducing the substitution $\beta = te^{j\theta}$ along with the even property of $F(\beta)$ we obtain

$$H(\alpha) = h(\theta - \theta_\alpha) \ln[F(\alpha)] + \frac{\alpha e^{j\theta}}{\pi j} \int_0^\infty \frac{\ln[F(te^{j\theta})]}{t^2 e^{j2\theta} - \alpha^2} dt, \quad (B6)$$

which presents a numerical difficulty when the pole at $t = \alpha e^{-j\theta}$ is near the real axis. This can be treated via an addition-subtraction process, provided $\alpha \notin C_2$. Specifically, we add and subtract to the numerator its value at $t = \alpha e^{-j\theta}$. By evaluating the additive term analytically, (B6) becomes

$$H(\alpha) = \frac{1}{2} \ln[F(\alpha)] + \frac{\alpha e^{j\theta}}{\pi j} \int_0^\infty \frac{\ln[F(te^{j\theta})] - \ln[F(\alpha)]}{t^2 e^{j2\theta} - \alpha^2} dt, \quad (B7)$$

where the integrand is now regular at $t = \alpha e^{-j\theta}$. This effectively reduces ε to the order of δ , increasing the range of allowed θ and thus eliminating the concerns noted in the previous paragraph.

A final obstacle to the numerical evaluation of $H(\alpha)$ is the infinite upper integration limit of (B7). This may be remedied via the change of variables [11] $v = \frac{2}{\pi} \arctan t$ to obtain

$$H(\alpha) = \frac{1}{2} \ln[F(\alpha)] + \frac{\alpha e^{j\theta}}{2j} \int_0^1 \frac{\ln \left[F \left\{ e^{j\theta} \tan \left(\frac{\pi v}{2} \right) \right\} \right] - \ln[F(\alpha)]}{\sin^2 \left(\frac{\pi v}{2} \right) e^{j2\theta} - \alpha^2 \cos^2 \left(\frac{\pi v}{2} \right)} dv . \quad (\text{B8})$$

The integral can now be easily evaluated especially if θ is chosen such that $F(v)$ exhibits a rapid decay as it increases from 0 to 1.

Expressions (B2) along with (B8) provide a complete prescription for factorizing an even function regular on the strip $|\tau| < \tau_+$ and the angular sectors $0 < \theta < \theta_0$, $\pi < \theta < \pi + \theta_0$. The integral in (B8) is over a convenient finite interval, and will be numerically tractable for $\delta_1 < \theta < \theta_0 < \delta_2$, provided $\theta \notin [\theta_\alpha + \epsilon, \theta_\alpha - \epsilon]$ if $0 < \theta_\alpha < \theta_0$ and the zeros of $F(\beta)$ are not too close

the origin. This allows a selection of θ such that the numerical accuracy of (B2) and (B6) is optimized. Additionally, care must be taken in defining the branch of the logarithm in (B8) so that

$\ln \left[F \left\{ e^{j\theta} \tan \left(\frac{\pi v}{2} \right) \right\} \right]$ remains continuous on the path of integration, eliminating a branch cut

contribution.